Adhesion of Latex Spheres to Giant Phospholipid Vesicles: Statics and Dynamics

Christian Dietrich, Miglena Angelova, Bernard Pouligny

J. Phys. II France 7 (1997) 1651–1682 NOVEMBER 1997, PAGE 1651

Adhesion of Latex Spheres to Giant Phospholipid Vesicles: Statics and Dynamics

Christian Dietrich ([1]), Miglena Angelova ([2]) and Bernard Pouligny ([1,*])

([1]) Centre de recherche Paul-Pascal, avenue du Docteur Albert-Schweitzer, 33600 Pessac, France
([2]) Institute of Biophysics, Bulgarian Academy of Sciences, 1113 Sofia, Bulgaria

(Received 24 February 1997, revised 23 June 1997, accepted 15 July 1997)

PACS.68.10.-m – Fluid surfaces fluid-fluid interfaces
PACS.62.20.Dc – Mechanical properties of liquids
PACS.87.22.-q – Physics of cellular and physiological processes

Abstract. — We studied the sequence of phenomena which occur when a solid microsphere is brought in contact with an isolated giant lipid vesicle. We used Latex beads, a few microns in diameter, which were manipulated individually by means of a long-working-distance optical trap. The evolution of the bead/vesicle system was characterized in time, from $\sim$ 1 ms to $\sim$ 100 s. In this time range, we identified different steps, namely adhesion, ingestion, expulsion and re-capture. In the adhesion step the sphere moves quickly in direction to the vesicle interior and the surface of the particle becomes wetted by lipids. We propose a simple model, based on the counter-balance between adhesion and stretching of the lipid lamella, which explains the experimental equilibrium configuration. The bead/vesicle configuration after the adhesion step pertains to partial or complete wetting, depending on the initial vesicle state. Partial wetting can be followed by a second step, which we named "particle ingestion", and which leads to complete (or nearly complete) wetting of the particle surface. Ingestion is characterized by a further penetration of the particle across the vesicle contour, in concomitance with a decrease of the vesicle size. The phenomenon is attributed to the occurrence of a dynamically stabilized pore across the membrane, which allows part of the water initially inside the vesicle to flow out. Ingestion can be followed by a back and forth movement (expulsion and re-capture) of the particle. In the ultimate configuration, the solid surface is totally wetted by lipids, however with a finite contact angle between the membrane and the solid surface.

Nomenclature

k_a	elastic surface expansion modulus
A	membrane-substrate adhesion energy density
σ	lateral membrane tension
R	vesicle radius
ε	relative surface area excess of vesicle
a	solid sphere radius
θ	contact angle
z	penetration value (dimensionless)
z_e	equilibrium penetration value (dimensionless)

(*) Author for correspondence (e-mail: pouligny@crpp.u-bordeaux.fr)

1. Introduction

Lipids in water assemble into aggregates of different structures, in particular, they form bimolecular layers. "Liposomes" are small vesicles whose membranes are made of one or several such bilayers. Recently, some methods [1,2] were developed for preparing "giant lipid vesicles" of sizes in the 10 to 100 μm range. Such vesicles, well visible in light microscopy, are ideal tools to study basic mechanical and hydrodynamic properties of lipid bilayers.

The academic interest in liposomes is due to a large extent to their potential to offer ultimately simplified models of biological cells. Knowledge of vesicle properties obviously helps understanding such phenomena as cell deformation, shape transformation, membrane inclusions mobility, membrane permeability, *etc.*

Membrane to membrane, or membrane to solid substrate adhesion is a great issue which has already motivated a large amount of work, either theoretical [3–5] or experimental [6, 7]. Usually, a distinction is made between the "weak" and the "strong" adhesion regimes [5]. Membrane tensions involved in the "weak" regime are small ($\sigma < 0.1$ dyne/cm) and the events are partially driven by thermally excited membrane undulations. This situation occurs in the case of a flaccid vesicle having a low energy of interaction with the substrate (for instance, an other membrane) [8]. "Strong" adhesion corresponds to large energies and tensions ($\sigma > 0.5$ dyne/cm). In this regime, membrane undulations are smoothed out. The problem is just mechanical and has much in common with the wetting of a substrate by a liquid droplet.

This article focuses on the interaction of lipid vesicles with the surface of solid spheres in the case of a particle (a few microns in diameter) which is definitely smaller than the vesicle (a few tens of microns in diameter). As in the above mentioned problems, the properties of the simple sphere/vesicle system may have some relevance to some biophysical problems, for example, to understand the way of penetration across the cell membranes for colloidal size entities. A basic knowledge in this field can even be very important to optimize drug vectorization based on microparticles [9].

An other motivation of this study is more at the mechanical engineering level, since microspheres attached to membranes have been used as "handles", for instance, for pulling tubular filaments [10], as force transducers [11] and as probes to measure lipid membrane viscosities [12].

This article contains a section on modelization and a larger experimental part. To summarize, the particles used in our experiments are common Latex microspheres, with negative surface charges (sulfate groups). The particles are manipulated by means of an optical levitation trap and brought in contact with spherical giant lipid vesicles in plain water (pH $\approx$ 5). Unless otherwise stated, the vesicles are isolated and unilamellar. Membranes are made of SOPC or DMPC, are in the fluid state and electrically neutral. Observations are carried out by means of optical microscopy, in phase or amplitude contrast. Essentially, we observe the position of the spherical particle relatively to the membrane, *i.e.* the degree of penetration of the sphere inside the contour of the vesicle, which is equivalent to defining an apparent contact angle of the membrane on the solid surface. Data are gathered at video rate (25 Hz), using standard image numerization. In a few experiments, the particle position was measured at a 1.1 kHz rate, by means of an analog position sensitive device.

As we will see, adhesion of a Latex particle on a vesicle pertains to the "strong adhesion" regime and always proceeds through a first step which can be described as a partial wetting of the solid surface by the lipid membrane. In this step, the vesicle behaves somehow as an emulsion droplet.

In Section 2, we set out a simple mechanical model to describe the sphere/vesicle equilibrium configuration in this situation. Although the basic concepts used in the model are not new (see for instance [4]), the specific problem that we address (a finite size particle interacting

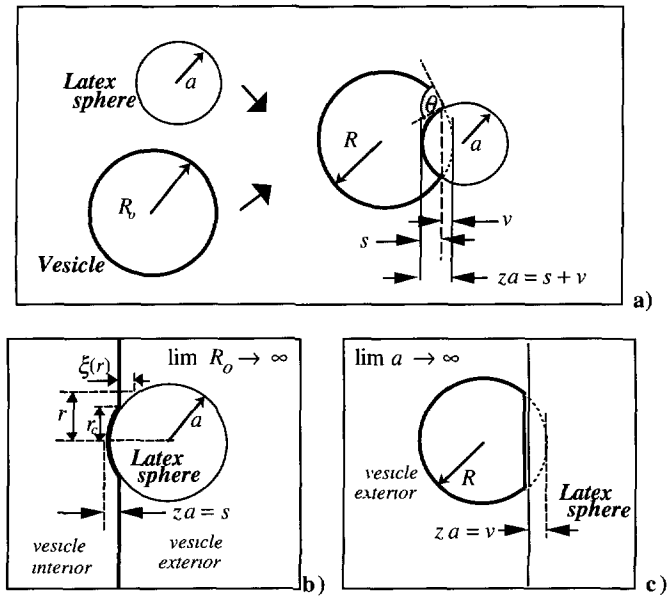

Fig. 1. — Geometry of solid sphere-lipid vesicle contact. a): General problem (finite a and R_0). Note that the vesicle radius is changed after contact. b): Adhesion of a solid sphere to an infinite plane lipid membrane. c): Adhesion of a vesicle to an infinite flat substrate.

with a finite size vesicle) was not discussed before us in details. Essentially, Section 2 is aimed at computing the degree and kinetics of penetration of the particle across the vesicle contour and the membrane tension at equilibrium.

The following sections are experimental. The materials and methods that we used are itemized in Section 3. Our experimental observations are reported in Section 4. We identify different steps in the sphere/membrane interaction: adhesion, ingestion, expulsion and re-capture. These different events are described in terms of particle position and vesicle configuration as a function of time.

These observations are analyzed in Section 5. We discuss the adequateness of the partial wetting picture to describe the adhesion step in the above sequence and estimate the value of the sphere/lipid membrane adhesion energy density. We also give an interpretation of the particle ingestion based on the creation of a dynamically stabilized pore across the membrane [13]. Some questions, essentially kinetics, are left unsolved and set out as open problems.

The main points of the paper are summarized in the final Section 6, together with prospects for future work. Some of the technical details of the calculations are explained in two appendices at the end of the article.

2. Theory

2.1. STATIC EQUILIBRIUM. — We consider the situation sketched in Figure 1a. We want to describe the geometry of the vesicle and solid particle complex at equilibrium, *i.e.* well after both entities have got in contact. This problem has some analogy and differences with the classical situation of the spreading of a liquid on a solid surface (wetting). In this case, the geometry of the complex is found from the Young equation, which gives the contact angle

(denoted θ in Fig. 1) of the liquid on the solid surface. We write the Young equation as:

$$\sigma(1 + \cos\theta) = A \tag{1}$$

$\sigma = \sigma_{LW}$ is the tension between the liquid (L) and the outer fluid – say water (W) and A is the adhesion energy density between the liquid and the solid (S). A can be defined in terms of interfacial tension as:

$$A = \sigma_{LW} + \sigma_{LS} - \sigma_{SW}. \tag{2}$$

The volume of liquid, $V = 4/3\ \pi R_0^3$, is conserved in the interaction. The final droplet radius R, depends on R_0, on the contact angle θ, and on the sphere radius, a. To summarize, the equilibrium configuration of the complex is found from 2 physical constants, A and σ, and from 2 input parameters, a and R_0. The problem can be complicated by the existence of an energy term related to the SLW contact line, which is usually taken as proportional to the length of contact line, independently of the contact angle. Whether this line energy is important in practical situations is a matter of controversy [14–16].

We come back now to the problem with the vesicle. Again we suppose that the volume V inside the vesicle is conserved in the interaction with the solid sphere, and define R_0 as $(3V/4\pi)^{1/3}$ We neglect entropic contributions to the membrane roughness and relate the lateral tension to the elastic expansion of the lipid bilayer. For the lipid species of interest, this is a very good approximation for lateral tensions $\sigma > 0.5$ dyne/cm. The membrane can then be viewed as an elastic sheet, characterized by a surface area at rest (zero tension) S_0 and by a constant expansion modulus k_a [17]. If $S_0 < 4\pi R_0^2$, the vesicle takes on a spherical shape of radius $R > R_0$. The elastic energy of the film reads:

$$E_{el} = \frac{1}{2} k_a \frac{(S - S_0)^2}{S_0} \qquad \text{(if } S_0 < 4\pi R_0^2\text{)}, \tag{3}$$

with $S = 4\pi R^2$. In equation (3), one implicitly supposes that the surface density is uniform in the membrane. For simplicity we will keep this assumption throughout this paragraph. The membrane tension is given by:

$$\sigma = k_a \frac{(S - S_0)}{S_0} \qquad \text{(if } S_0 < 4\pi R_0^2\text{)}. \tag{4}$$

If S_0 is larger than $4\pi R_0^2$, the membrane does not need to be compressed. To accommodate the excess surface area, $S_0 - 4\pi R_0^2$, the vesicle takes on a non-spherical shape. If the relative surface excess $\varepsilon = (S_0/4\pi R_0^2) - 1$ is small, the vesicle is quasi spherical.

We suppose now that the bilayer adheres on the surface of the solid sphere, and that this surface is partially wetted by phospholipid much in the same way as in the case of the liquid droplet. In general, this process increases the membrane surface area. The exception to this rule is when the initial excess area is larger than $S_0 - 4\pi a^2$, *i.e.* when $\varepsilon > (a/R_0)^2$. In this case the particle is completely wrapped by the membrane, with no cost in elastic energy. If $\varepsilon < (a/R_0)^2$ the final shape of the vesicle outside of the contact region is spherical. Equation (1) is still valid, but it does not give the value of the contact angle directly, because σ is not a constant. Here the physical constants are A and k_a, and the input parameters are a, R_0, and ε. The configuration of the system is found by minimizing the total energy

$$E = E_{el} + E_{ad} + E_l \tag{5}$$

with the constraint of volume conservation, V = constant.

$$E_{ad} = -AS_{ad} \tag{6}$$

is the energy gained in adhering the membrane on the solid surface. S_{ad} is the membrane/solid contact surface area. E_l is a line energy term, which comes from the fact that the curvature of the membrane along the contact line cannot be infinite. We will skip this term in the following, because it is negligible small in the conditions of our experiments. We justify this point in Appendix A. Briefly, we find that the ratio of the line energy term to the surface energy terms in equation (5) is on the order of $\sqrt{k_c/k_a}(R_0/a^2)$, where k_c is the curvature elastic constant of the membrane. With $k_c \approx 10^{-13}$ erg, $k_a \approx 200$ erg/cm^2, $R_0 = 30$ μm, $a = 8$ μm, we find that the line energy contributes only a 10^{-3} fraction of the total energy.

Thus we may keep only E_{st} and E_{ad} in equation (5). As with the liquid droplet, the variables θ and R_0 can be used to define the configuration of the system. Instead of θ, we chose the variable z, which represents the interpenetration of the vesicle and solid sphere contours (see Fig. 1). For convenience, the interpenetration length is defined as za, which makes z a dimensionless number. Actually, z is the parameter which is most directly felt by the experimentalist in the real situation. The following formulas will be deduced for the case when the sphere is much smaller than the vesicle (*cf.* Fig. 1; $(a/R) \to 0$ limit). In this case the curvature of the membrane and the increase of the vesicle radius due to the sphere segment penetrating into the vesicle can be neglected. This will allow us to develop all relevant features of the scenario without the need of an extensive mathematical treatment. For the materials of interest in this work, this simplified consideration gives a reasonable description of the partial adhesion, for values of a/R_0 smaller than about 0.3. This is demonstrated in Appendix B, where the rigorous numerical solution is given for any combination of sphere and vesicle radius. When $R_0 \gg a$ (Fig. 1b), we simply have:

$$z = 1 + \cos\theta. \tag{7}$$

Moreover, the variation in the vesicle volume due to the penetration of the sphere is negligible, which allows us to drop the constraint of volume conservation. Simple geometry gives:

$$S - S_0 = \pi a^2 z^2 - 4\pi R_0^2 \varepsilon \tag{8a}$$

$$S_{ad} = 2\pi a^2 z, \tag{8b}$$

which we inject into equations (3, 6, 5). The equilibrium penetration z_e is found from $dE/dz = 0$, which gives:

$$k_a \left[\left(\frac{a}{2R_0} \right)^2 z_e^3 - \varepsilon z_e \right] = A. \tag{9}$$

Note that, with the definitions of z and σ (Eqs. (7 and 4), respectively), equation (9) is just a version of the Young equation (Eq. (1)). Equation (9) expresses the balance between the elastic force

$$f_{el} = -2\pi a k_a \left[\left(\frac{a}{2R} \right)^2 z^3 - \varepsilon z \right] \tag{10a}$$

and the adhesion force,

$$f_{ad} = 2\pi a A. \tag{10b}$$

Figure 2 shows the calculated adhesion and elastic forces for different sets of assumed adhesion energy densities A and relative surface excess areas ε, for a size ratio $a/R_0 = 0.2$. We took $k_a = 200$ dyne/cm, the value reported for SOPC bilayers [18]. DMPC membranes have a slightly lower k_a (≈ 145 dyne/cm [18]). but this does not make a great difference in our numerical results. The different equilibrium penetration values z_e are determined graphically from the intersection of $-f_{el}(z)$ and $f_{ad}(z)$ curves. Dotted lines correspond to the $R_0 = \infty$ approximation, *i.e.* to equation (10), while solid lines represent the exact numerical solution

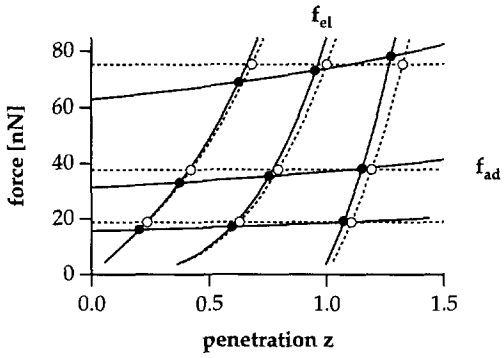

Fig. 2. — Plots of the adhesion (f_{ad}) and dilatation ($-f_{el}$) forces *versus* the particle penetration (z), for a size ratio $a/R_0 = 0.2$. Dashed curves are the result of the $R_0 \to \infty$ approximation. In this limit, $f_{ad}(z) = 2\pi aA$ (Eq. (10b)) is just a horizontal line. The three lines, from top to bottom, correspond to $A = 2, 1$ and 0.5 erg/cm^2, respectively. The tilted dashed lines are $-f_{el}(z)$ graphs following equation (10a), with $k_a = 200$ dyn/cm and $\varepsilon = -1\%$, 0%, $+1\%$, from left to right. The solid lines are the exact (numerically computed) graphs, with the same input parameters. The equilibrium penetration is found from the intersection of the $f_{ad}(z)$ and $-f_{el}(z)$ graphs. Approximate ($R_0 \to \infty$) solutions are shown as open circles, and exact solutions as bold circles.

(*cf.* Appendix B). Clearly, the error due to the approximation, *i.e.* the influence of volume conservation, is rather small for this size ratio.

Figure 3 shows the values of z_e and of the membrane tension σ for different values of a/R_0, A and ε, calculated with the numerical procedure. We observe that, for a given vesicle (R_0, ε) and adhesion energy (A), the penetration z_e decreases and the tension σ increases when the sphere size increases. The singularity along each curve comes from the fact that z_e has to be smaller than 2. The left branch corresponds to complete wetting ($z_e = 2$), *i.e.* the particle is totally encapsulated by the membrane. In the limit $R_0 \to \infty$, total encapsulation demands $A \geq A_e$, with:

$$A_e = 2k_a[(a/R_0)^2 - \varepsilon] \qquad \text{(total encapsulation energy, } R_0 \to \infty). \tag{11a}$$

In this regime, the membrane tension is given by:

$$\sigma = k_a \left[\left(\frac{a}{R_0} \right)^2 - \varepsilon \right] \qquad \text{(total encapsulation, } R_0 \to \infty). \tag{11b}$$

The right branch of each curve corresponds to partial wetting or encapsulation. For $\varepsilon = 0$, one finds from equations (4 and 9):

$$\sigma = k_a^{1/3} A^{2/3} \left(\frac{a}{2R_0} \right)^{2/3} \qquad \text{(partial encapsulation, } R_0 \to \infty). \tag{12}$$

At the transition point, the tension takes on the value $\sigma* = A/2$. Note that this result is a direct consequence of the Young equation (Eq. (1)) and therefore has to be valid for any value of a/R_0 (*cf.* Appendix B).

We recall that this model is purely mechanical in that it ignores the part of the membrane tension which is driven by thermal undulations [17]. Taking the entropic contribution to

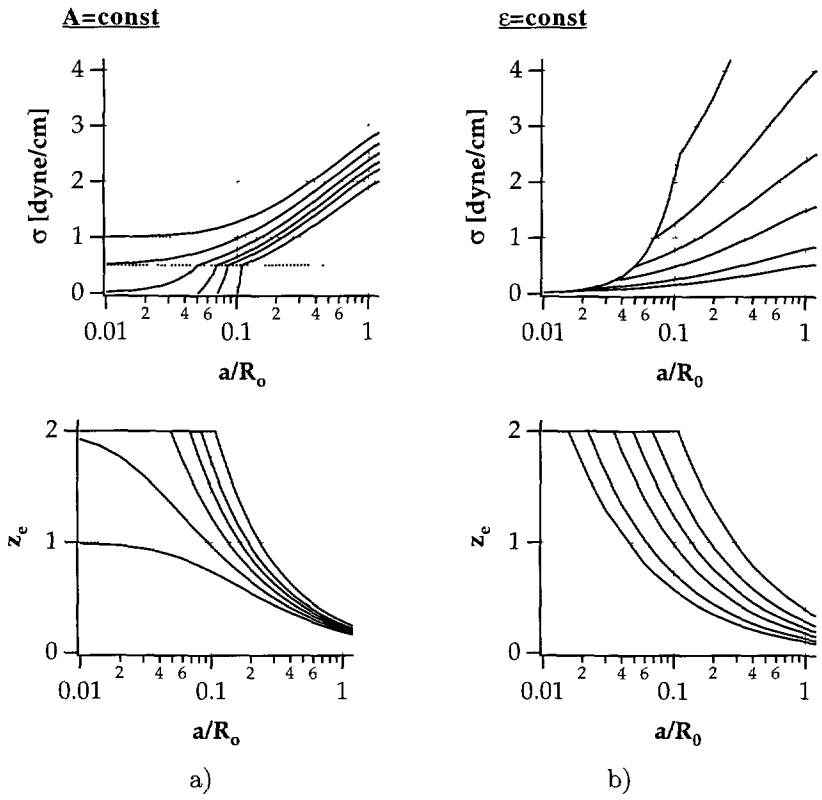

Fig. 3. — Numerically computed graphs of the membrane tension (σ) and sphere equilibrium penetration (z_e) *versus* size ratio (a/R_0). In panel a), A is taken = 1 erg/cm^2, while ε is varied: $\varepsilon = -0.5$, -0.25, 0, 0.25, 0.5, 1%, from bottom to top. k_a is taken everywhere = 200 dyne/cm. In panel b), the initial excess area (ε) is chosen = 0; the different graphs correspond to A = 0.1, 0.2, 0.5, 1, 2, 5 erg/cm^2, from bottom to top.

membrane elasticity into account leads to large deviations in the plots of Figure 3, in the region where the tension after the adhesion step is smaller than 0.5 dyne/cm (data not shown). As to expect, in this regime the drop in tension with decreasing values of a/R is less drastic than indicated by Figure 3 plots. Because of this, the penetration values shown in the lower panels of Figure 3 are over-estimated. This is due to thermal undulations, which keep the bilayer under lateral tension. As we will see, A is estimated on the order of 1 erg/cm^2 in our experiments, which leads to $\sigma* \approx 0.5$ dyne/cm. Therefore the tension for a partially encapsulated sphere in our experimental situation is well in the mechanical (or "strong" adhesion) regime, as we assumed.

The curves in Figure 3 can be used to interpret the experimental sphere-membrane configurations and for testing the model. An obvious feature of these curves is the non-constancy of the tension, which makes the problem qualitatively different from that of wetting of a solid by a liquid droplet. An other specificity of the vesicle membrane is that it may rupture when σ exceeds some value σ_c, which is on the order of a few dyne/cm [18]. The calculations indicate that such amplitudes can be reached with energy densities on the order of an erg/cm^2.

2.2. ENCAPSULATION DYNAMICS. — In this paragraph, we want to make some prediction about the dynamics of particle encapsulation based on the partial wetting picture. Essentially, we will just adapt the theory that describes the spreading of a liquid droplet on a solid surface in the partial wetting regime [19,20].

In the simple case when the third phase is a vapor and the liquid is non volatile. dissipation comes just from the flow gradient in the liquid wedge near the contact line. In our situation, both sides of the moving interface are made of water, and therefore we have two such wedges. To keep the description simple, we will consider only small penetrations ($z \ll 1$). In this case, which corresponds to a very large contact angle ($\theta \cong \pi$) we expect large flow gradients essentially in the wedge between the membrane and the non wetted part of the solid surface. We may then restrict the calculation of the dissipated power, P, to this region.

The situation of interest is sketched in Figure 1b. We denote r the distance to the figure symmetry axis (which passes through the particle center). We suppose the membrane approximately flat, *i.e.* $R_0 \gg a$. We define $\xi(r)$ as the thickness of the wedge at distance r. In the limit of a small penetration, the radius of the contact line is given by $r_c = (2za^2)^{1/2}$ Of course, $\xi(r_c) = 0$. We denote x the distance to the membrane in the wedge: $0 \leq x \leq \xi$.

We suppose that the sphere is fixed and that the membrane moves up to wet the particle surface. For small penetrations, the wedge is very narrow and we may consider that the flow velocity $\mathbf{u}$ is everywhere perpendicular to the symmetry axis (lubrication approximation). Following Charles and Mason [21], we write:

$$u(x,r) = U(x,\xi)\psi(r) \tag{13}$$

U is a second order polynomial in x, whose coefficients are determined by the boundary conditions: (i) $u = 0$ on the solid surface ($x = \xi$); (ii) $u = u_m$ on the membrane ($x = 0$). Here u_m is the material velocity of the membrane, and is found from the mass conservation condition, $2\pi r u_m = \mathrm{d}S/\mathrm{d}t$. This gives:

$$u_m(r) = \frac{a^2}{r} z\dot{z}. \tag{14}$$

We thus find:

$$u(x,r) = x\psi(r)[\xi(r) - x] + u_m(r)(1 - \frac{x}{\xi(r)}). \tag{15}$$

An explicit expression for $\psi(r)$ is found from the condition of incompressibility of the fluid in the wedge. Again following reference [21], we consider the volume between r and $r + \mathrm{d}r$, *i.e.* $\delta v = 2\pi r \mathrm{d}r\psi(r)$ and the flux $Q = 2\pi r \int_0^\xi u(x,r)\mathrm{d}x$. Because the membrane moves up, δv varies in time. This variation is compensated by the variation of Q between r and $r + \mathrm{d}r$. This balance leads to:

$$\psi(r) = \frac{3a^2}{r\xi^2(r)}\dot{z}(2 - z). \tag{16}$$

With the full expression of $u(x,r)$ now at hand, we can calculate the power dissipated in the wedge, which is given by:

$$P = \eta \int_{r_{min}}^{r_{max}} 2\pi r \mathrm{d}r \int_0^\xi \left(\frac{\partial u}{\partial x}\right)^2 \mathrm{d}x, \tag{17}$$

where η is the fluid viscosity. r_{max} is a large scale cut-off, on the order of the sphere radius. In fact, it is not necessary to know r_{max} precisely, because P is determined essentially by the divergence of $\partial u/\partial x$ near the contact line. Because of this divergence, we impose a lower limit

l to ξ, on the order of a molecular size. This restricts the integration in equation (17) to $r \geq r_{\min} = r_c + l/\sqrt{2z}$. This yields:

$$P \approx 4\pi\eta a^3 \frac{\dot{z}^2(3 - 3z + z^2)}{z} \ln\left(\frac{a\sqrt{2z}}{l}\right). \tag{18}$$

Equation (18) is valid for $za \gg l$, *i.e.* for penetration depths much larger than a molecular size.

The dissipated power is balanced by the work per unit time done by the adhesion and elastic forces acting on the membrane:

$$P = -\mathrm{d}E/\mathrm{d}t \tag{19}$$

with

$$\mathrm{d}E/\mathrm{d}t = -2\pi a^2 \dot{z}(A - \sigma z) \qquad (\text{for } R_0 \to \infty). \tag{20}$$

The equation of motion is then:

$$\dot{z} = \frac{A}{6\eta a \ln(a\sqrt{2z}/l)} \, z \, \frac{1 - z\sigma/A}{1 - z + z^2/3}. \tag{21}$$

Equation (21) gives an analytical solution for our model in the limit of $a/R_0 \to \infty$. It can be cast in the more general form:

$$\dot{z} \approx \frac{z\mathrm{d}E/\mathrm{d}z}{(3 - 3z + z^2)4\pi\eta a^3 \ln\left(\frac{a\sqrt{2z}}{l}\right)}. \tag{22}$$

The penetration velocity ($\dot{z}$) starts from zero at the onset of adhesion because the wedge is infinitely narrow when $z = 0$ (P diverges). Integration of equation (22) (or Eq. (21)) leads to a characteristic S-shaped trajectory. An example of encapsulation dynamics which we computed from equation (22) is displayed in Figure 7c (solid line), for comparison with an experimental record (details are given in Sects. 3 and 4). The Figure shows the real displacement $d(t) = d(0) - z(t)a$ of the Latex bead relatively to the vesicle, in correspondence with the experimentally recorded signal (see Sect. 4). In this example, $a = 7.7$ μm, $R = 19$ μm. We took $\varepsilon = 0$, and adjusted A (here $A = 0.8$ erg/cm^2), to make $d(t \to \infty)$ coincide with the experimental value. The cut-off l was chosen equal to 1 nm. Of course, l does not need to be precisely defined, because it appears only in a logarithm. The computed curve starts at some initial penetration ($z_s > 0$), whose value can be chosen rather arbitrarily. In practice, z_s has to be much larger than a molecular length, and can be taken on the order of the minimum displacement that can be experimentally detected.

The encapsulation time τ_{enc} may be defined as the time elapsed between, say, 0.1 z_e and 0.9 z_e In this example, $\tau_{enc} \approx 1.8$ ms. Note that the lubrication approximation makes sense only for small values of z. Consequently the asymptotic regime of $z(t)$ is probably poorly described by the model. As a whole, we may just retain our estimate that A on the order of an erg/cm^2 leads to τ_{enc} on the order of a millisecond.

3. Materials and Methods

3.1. Sample Preparation. — Giant vesicles, a few 10 microns in size, are generated by the method of electroformation [1,2]. All preparations are made directly in the glass chamber used for manipulation by laser beams (Fig. 4). This chamber (THUET optical cell) has a 1 mm optical path and is equipped with two parallel cylindrical (Ø 0.8 mm) platinum electrodes.

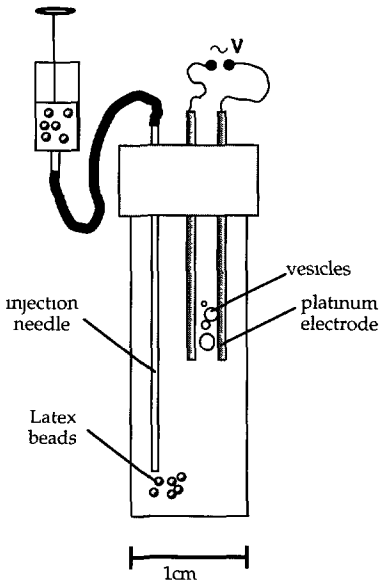

Fig. 4. — Scheme of the sample chamber. Note: for clarity, spheres and vesicles are not to scale.

The separation (axis to axis distance) between the electrodes is about 3 mm. We used L−α−dimyristoyl phosphatidylcholine (DMPC; Avanti Polar Lipids) or L−α−stearoyl−oleoyl−phosphatidylcholine (SOPC; Avanti Polar Lipids) which were swollen in pure water (MILLIPORE milliQ). SOPC membranes are fluid at room temperature. Experiments on DMPC membranes were carried out in the fluid state too. For this reason, the temperature of DMPC samples was adjusted well above 30 °C by means of an Indium Tin Oxide (ITO) covered glass slide in contact with the chamber. The conducting layer was connected to a thermostat (TC) which regulates the temperature by sending current pulses of different length through the ITO layer. The thermoresistance located inside the chamber yields the feedback signal. As usual in the electroformation method, an AC field is applied to the electrodes, to generate a cluster of vesicles in contact with platinum. Giant vesicles are found at the periphery of the cluster. These vesicles are not ideal samples for experimenting, because they are interconnected, and consequently the topology of the membrane is not known exactly. Fortunately it usually happens that a few vesicles disconnect from the cluster spontaneously. This process takes place a few hours (up to a few days) after formation of the vesicle cluster. "Free" vesicles are easily identified by the fact that they can be moved on arbitrary distances by convection, in practice by gentle injection of water into the cell. Conversely, vesicles attached to the cluster can be moved only on short distances and come back to their original position after the injection has been stopped.

For adhesion experiments we used Latex spheres with diameters in the range between 2 and 20 μm provided by Polysciences. We do not know the charge density on the sphere surface. We just estimated the surface potentials of individual spheres in the 12 to 20 μm diameter range and found −80 mV as an average [22]. From the stock solutions (Polybeads Polystyrene Microspheres, 2.5% solids in deionized water) we made very diluted suspensions in milliQ water (conc. 0.02% solid) which were then injected into the chamber *via* a small stainless steel needle, whose tip was about 20 mm apart from the electrodes (Fig. 4). The injection rate was chosen small enough to avoid damage of the vesicles. In typical conditions, we were able to optically

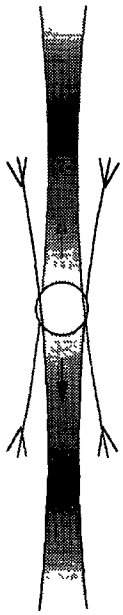

Fig. 5. — Geometry of the two-beam laser trap. The gray values illustrate the amplitude of the radiation pressure along the z-axis. The sphere is trapped between the two "dark" regions.

catch an injected sphere "in flight" very near to the tip of the injection tube. The trapped sphere was then transported towards the electrodes, where a vesicle was selected to produce a contact. Special care was taken to avoid any pollution of the sphere surface with lipid molecules before the first contact with a lipid membrane.

3.2. OPTICAL SET-UP. — Manipulation of Latex spheres is performed by means of an optical trap fairly similar to Buican's original design [23]. For a detailed description, see Angelova and Pouligny [24]. Briefly, the glass chamber (Fig. 4) is held horizontally inside the optical levitator. Its position in horizontal directions (x, y) is controlled by means of motorized stages (Unidex 11, Aerotech). The vertical position (z) is tuned manually. For the purpose of the present report, it suffices to know that two vertical counter propagating coaxial laser beams are focused inside the cell by means of two microscope lenses. In the same time, these lenses are part of a classical microscope for observation of the sample. The source feeding the set-up is a continuous wave argon ion laser. Compared to the now widespread "optical tweezers" design [25], our set-up has the disadvantage of being more complex, but offers a much longer working distance ($\geq$ 4 mm), and lower power densities in the sample ($< 10^5$ W/cm^2 in our experiments). The beam-waists of the two beams are slightly separated longitudinally to build a small region where a sphere can be stably trapped (Fig. 5). The forces acting on the trapped particle have been studied in details elsewhere [26]. There is no detectable laser induced heating of the particles in bulk water. Forces are due to radiation pressure. The horizontal force can be varied from about 1 to 100 pN in our conditions. For microscope observation, the lower objective (LD Epiplan 50 × /0.5 ∞; Zeiss) is employed as a condenser while the upper one (LD Achroplan 40 × /0.6∞; Zeiss) is the observation objective. Images are captured by a CCD camera (C2400, Hamamatsu) and recorded by standard video equipment. Phase contrast is well-suited for observing the vesicles (the vesicle contour shows up as a sharp dark line) but is

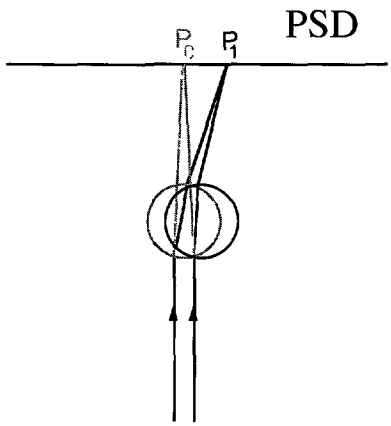

Fig. 6. — Principle of measurement of the sphere excursion by means of the position sensitive detector (see Sect. 3).

rather inconvenient to visualize the Latex spheres (images are complex interference patterns, see Fig. 7). For this reason we sometimes switch the system to amplitude contrast, which is better to visualize the particle contour. Usually the optical trap and then the particle is held fixed in space. We move the chamber to bring a vesicle in contact with the particle.

3.3. Digital Image Processing. — We used a commercial image processing system installed on a Digital Workstation (DEC 3000/Axp 600 equipped with a J300 board). A home written software program (Language C++) allowed us to save digitized frames at video frequency and 8 bit resolution on the hard disk. The same program was used to load single frames and to determine vesicle contours and bead positions. Because of the bright image of the Latex spheres, a tracing algorithm for detecting the vesicle contour is hardly applicable. We helped ourselves by determining six points on the vesicle contour by hand and subsequently by fitting a circle to these points. The procedure provides the position and radius of the vesicle (within $\pm$ 0.5 μm) and was applied in an analogous way for determining the position of Latex spheres. The radius of the Latex sphere was determined separately, prior to the collision with the vesicle. In each case, we measured the sedimentation velocity of the particle in bulk water. Knowing the Latex density (1.05 g/cm^3) and the water viscosity ($\eta = 0.01$ poise), this procedure allowed us to deduce the particle radius within $\pm$ 0.2 μm. Calibration of the pixel resolution in x and y direction revealed that one pixel corresponds to an area of 0.154 μm $\times$ 0.162 μm on the specimen.

3.4. Position Sensitive Detector. — As explained in the following section, particle displacements in the first adhesion step happens much faster than the video rate. To resolve this displacement in time we set up a procedure based on the deflection of the levitation laser beam. As shown in Figure 6, when the sphere moves horizontally, the laser beam is deflected laterally. The method amounts to measuring the excursion of the laser cross section in a horizontal plane (P) located at some distance (20 μm) above the sphere. In reality, we picked-up the small amount of green light (1 mW) that goes through the observation system and built a real image (P$'$) of (P) in a separate arm near the video camera [22]. The excursion of the laser spot was measured in (P$'$) by means of an analog position sensitive detector (PSD C4674, Hamamatsu). This device yields two signals proportional to the coordinates of the spot in (P$'$), with the zero

taken at the center of the PSD photosensitive area. The output signals (x and y) of the PSD were digitized by an AD converter (PC-LPM-16, National Instruments). The response time of the detector and connected AD converter was checked to be clearly shorter than 0.1 ms. A commercial software package (Testpoint Version 1.1c, CEC) allowed for the recording of the sampled data points at a rate up to 1100 Hz.

We used this method with particles of diameter $2a \approx 15$ μm. We made tests by means of calibrated displacements d of the particles horizontally (this was done by moving the cell by means of the motorized stage, while the trap was switched off). We found that the signal $V(d)$ was proportional to the particle displacement d provided that $d < a$. Calibration was performed for every sphere separately. 20 mV/μm was a typical value of $V(d)/d$. The signal noise (standard deviation of the detector signal when a sphere is trapped) was about 3 mV.

Using the same system, we determined the stiffness (k) of the optical trap for each particle. When the laser is switched on, the particle moves back towards the beam axis under the action of the transverse optical force $f_\perp(d) \approx kd$. The trapped sphere can be described as a highly damped harmonic oscillator. The inertia effect can be neglected and the distance $d(t)$ decreases exponentially in time. k was determined from the characteristic time of this movement, $\tau = \xi/k$ where ξ is the Stokes friction coefficient ($\xi = 6\pi\ \eta\ a$) of the particle in water. The measured values of k (for instance $k = 2$ pN/μm for $a = 6$ μm) were in fairly good agreement (within 20%) with those computed using the generalized Lorenz-Mie theory [27]. In the experiments with vesicles, the excursion of the solid particle, as given by the PSD, was not exactly equal to the penetration length $az(t)$, because both the particle and the vesicle move when adhesion happens. From the video recordings, we determined that $d_v/d \approx a/R$ at equilibrium (d_v is the vesicle displacement at equilibrium). We supposed that this property was valid at any time, *i.e.* we used the correction $az(t) = d(t)(R + a)/R$.

3.5. NUMERICAL CALCULATION. — Numerical calculations were performed on a Macintosh computer (Macintosh, PowerBook 180) with a software environment for data graphing and data analysis (Igor Version 1.2, Wavemetrics). For numerical integration of differential equations, we used a Runge-Kutta algorithm of fourth order with step width control [28].

4. Results

As we will explain throughout this section, the solid sphere-vesicle interaction features different steps, namely *adhesion, ingestion, expulsion* and *re-capture.*

4.1. ADHESION. — ① is the event which takes place when the sphere gets in contact with the surface of the lipid membrane. This is achieved by optically manipulating the particle near the vesicle, a few microns from the outer surface. Then this distance is slowly decreased, until adhesion happens. At this stage, the particle makes a horizontal jump out of the optical trap in the direction to the vesicle interior. This event is illustrated by the video sequences of Figure 7a, which shows two examples for the adhesion event. The positions of the sphere immediately before and after adhesion are seen on the same frame (second frame in each row), which means that the event is definitely shorter than a video period (40 ms). The graphs in Figure 7b show the distance d between the sphere and vesicle centers and the radius R measured from the video recording in the second example. Characteristic for this event, no change in the vesicle radius could be detected, while the discontinuity in d at frame 36 clearly indicates the onset of adhesion (denoted ① in the graph). Figure 7c is a high temporal resolution version of the same event recorded by means of the position sensitive detector. Here the characteristic time τ_{enc} is about 4 ms. Other measurements in similar conditions gave values on the order of a

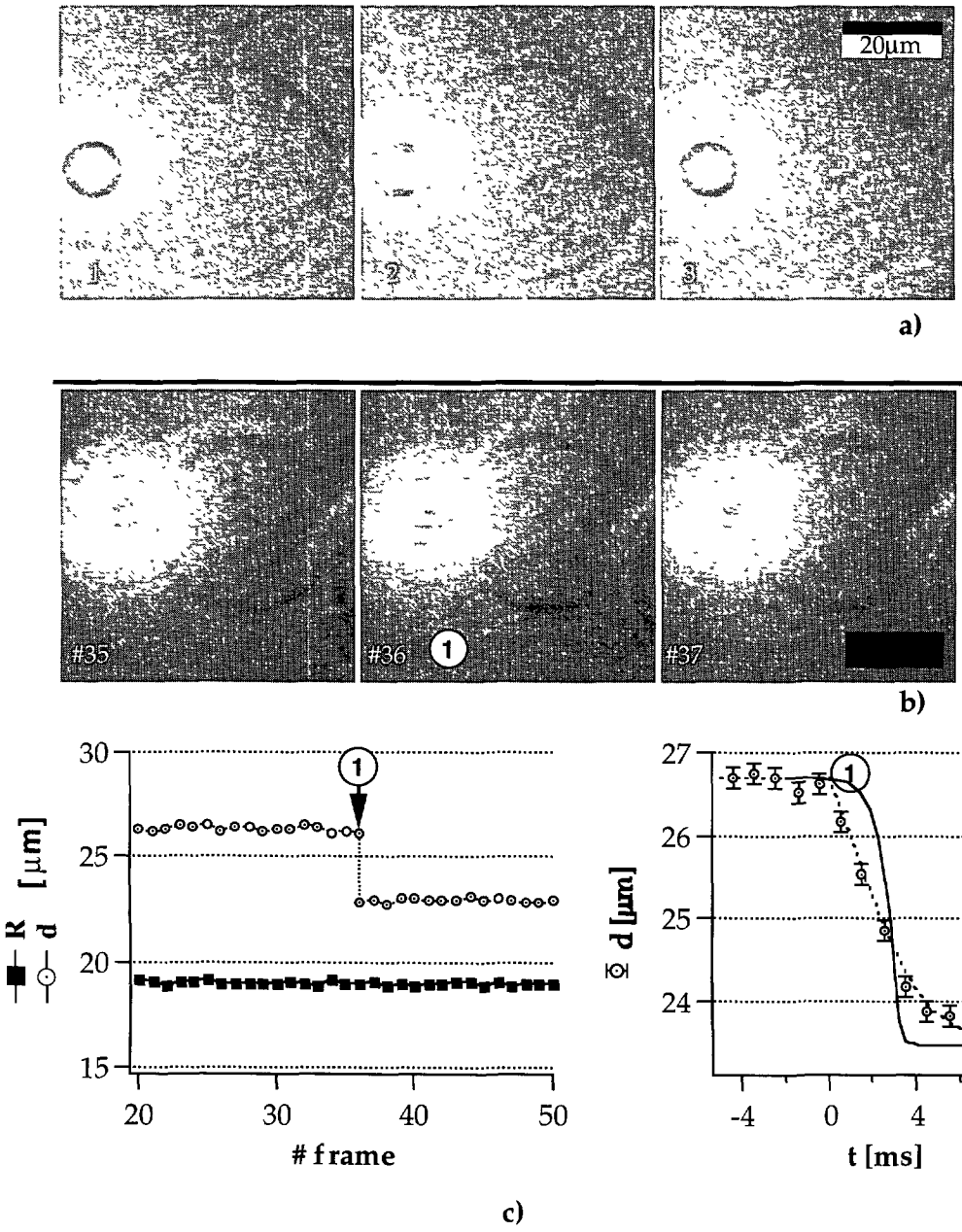

Fig. 7. — a) Two examples of an "adhesion" step of a Latex sphere onto a SOPC vesicle ($T = 24$ °C). First row: $a = 6.85$ μm, $R_0 = 22.4$ μm. Second row: $a = 7.7$ μm, $R_0 = 19$ μm. Time interval between subsequent frames was 40 ms. b) The graphs correspond to the second example: vesicle radius ($R(t)$, bold squares) and distance between vesicle center and sphere center ($d(t)$, open circles) for the whole video sequence. Note: frame numbers correspond to the number within the video sequence. c) The same event recorded with the PSD. Sampling rate: 1000 Hz. The error bars represent the standard deviation of the detector signal. The solid line corresponds to paragraph 2.2 theory, and the dashed line to the *ad hoc* (constant friction) model (see Sect. 5).

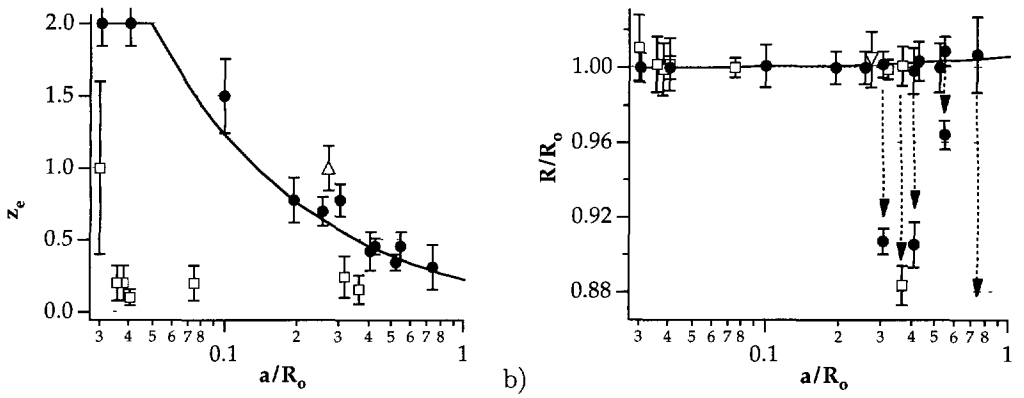

Fig. 8. — Analysis of the experimental equilibrium penetrations of Latex spheres into isolated unilamellar giant SOPC vesicles (T = 24 °C), for different values of the size ratio (a/R_0). Bold circles correspond to vesicles which were initially spherical (no visible thermal fluctuations), the triangle to one which was flaccid ($\varepsilon > 0$), and squares to vesicles which were pre-tensioned by means of an already adhered sphere. a) Measured penetration depth after adhesion step. The solid line represents the computed penetration depth for: k_a = 200 dyne/cm, A = 1 erg/cm^2 and ε = 0. b) Ratio of vesicle radii R/R_0 after and before sphere adhesion. The solid line corresponds to the trace in panel a). Each configuration which led to ingestion is marked with an arrow, whose tip points to the final value of R/R_0 (*cf.* Tab. I).

few milliseconds too. The radial velocity $\dot{d}(t) = a\dot{z}(t)$ changes instantaneously from 0 to about 1 μm/ms (within the resolution of the detection) and slows down to zero when the sphere has reached its equilibrium position.

At this stage, it is important to realize that the existence of an adhesion between the lipid membrane and the Latex particle is not influenced by the laser beams. We checked this several times by bringing a particle at some distance (about 20 μm) above a vesicle and then by switching off the laser trap. We observed that the particle would fall down, hit the surface of the vesicle, glide down for a few seconds, and make a characteristic brutal jump towards the vesicle interior, exactly in the way we just described.

After adhesion, the solid sphere can still be manipulated and moved by means of the optical trap. With partially encapsulated spheres ($z < 2$), as in the examples shown in Figure 7, the particle could be brought to any point on the surface of the vesicle, as one might expect since the membrane is fluid. In this kind of manipulation, the particle was moved relatively to the membrane. Indeed, when internal structures (or even other particles) were attached to the vesicle membrane, we could check that the manipulated particle did move relatively to these structures, which proved that the vesicle did not move as a whole. Movement transverse to the membrane is impossible with optical forces ($\leq$ 100 pN)), which means that the membrane-solid surface contact angle, or penetration degree z_e, is experimentally defined independently of the optical trap or of the particle weight. Pulling the particle with the optical trap in the direction opposite to the vesicle center makes the sphere-vesicle complex move as a whole. Interestingly, this is a further test that the selected vesicle was free. Moreover hydrodynamic drag brings the vesicle and sphere centers in the same horizontal plane automatically, perpendicular to the observation direction. This makes the top view of the sphere relatively to the vesicle free of parallax error, a condition which is required for a correct evaluation of the penetration.

Figure 8 shows the results from experiments performed with unilamellar SOPC vesicles, following the criteria described in Section 3. Bold circles correspond to vesicles which were

initially spherical, *i.e.* did not show shape fluctuations. The solid line is an adaptation of the theory set out in Section 2. Assuming $\varepsilon = 0$ and $A = 1$ erg/cm^2 reproduces the measured values well. The same figure shows an example of a vesicle which initially was slightly fluctuating (triangle), *i.e.* had a finite amount of excess area ($\varepsilon > 0$). Clearly the adhesion of the particle led to tensioning of the membrane, as the thermal fluctuations were suppressed instantaneously. The particle penetration is larger than in the former situation for the same a/R_0 ratio, as expected.

We performed a few experiments with 2 or more spheres which we successively adhered to the same vesicle. The squares in Figure 8a represent the penetration of the spheres, following the adhesion of a first sphere. Here the penetration is always smaller compared to those of single spheres. This behavior is well in line with what we might expect too, since the presence of the first sphere increases the membrane tension ($\varepsilon < 0$).

If the adhesion of the lipid membrane on the Latex spheres surface was reversible, one might expect that the penetration of the first sphere (z_1) be diminished when the second one is adhered to the vesicle. In the $R_0 \to \infty$ limit, we expect $z_{1,2}^{(2)} < z_1^{(1)}$ Here, the subscript refers to particle 1 or 2, and the superscript refers to the situation when one ((1)) or two ((2)) particles are attached to the vesicle. As far as we can decide (measuring all the above mentioned z's is a complex manipulation), experiments do not confirm the predicted two-sphere behavior. z_1 is not significantly modified when the second sphere is adhered to the vesicle. Instead we found $z_1^{(2)} \approx z_1^{(1)}$ and $z_2^{(2)} < z_1^{(2)}$ Apparently, adhesion of lipids on the particle surface is connected with a hysteresis effect.

Within the resolution of the measurement, the radius of the vesicle stayed unchanged (see Fig. 8b). This does not contradict our assumption that the vesicle internal volume is conserved. Indeed we expect an increase in the vesicle radius after particle adhesion, but the effect is small. The solid curve in Figure 8b shows the computed values of R/R_0 corresponding to the solid line in Figure 8a. Clearly, for the adhesion step the predicted variation in R is within experimental error.

In the simple "partial-wetting" picture, the portion of the solid sphere which is external to the vesicle contour is supposed to be "dry", *i.e.* free of lipids in our situation. Therefore it should be possible to adhere this outer portion to an other vesicle. We verified this by dragging a vesicle-sphere complex and colliding the "clean" portion of the sphere against a second vesicle. The result of such a manipulation is shown in Figure 9. As expected, a second adhesion followed, resulting in a "twin configuration". The procedure could be repeated, as long as a "dry" portion on the particle surface was available to connect a further vesicle. Such vesicle-sphere complexes could be optically dragged in water. In such experiments, we observed that the complex was oriented by the water flow (as one might expect for a non isotropic shape), but behaved as a rigid body: the vesicles stayed spherical and did not move relatively to each other. Note that this behavior does not contradict our statement that the solid sphere can move along the membrane to which it is attached. This just means that the membrane contact lines are "pinned" to the Latex surface. Of course this contact line pinning must be understood keeping in mind the magnitude of the forces involved during a manipulation: the optical forces (< 100 pN) acting on the solid sphere are not strong enough to make the lipids glide along the Latex surface.

Qualitatively the trends observed with SOPC vesicles were the same with DMPC vesicles at 30 °C. Apparently, the adhesion energy of Latex spheres on DMPC membranes is on the order of an erg/cm^2 too. We cannot be more accurate now, because the number of experiments which we performed with unilamellar DMPC vesicles (see Tab. II) is too small to provide reliable statistics.

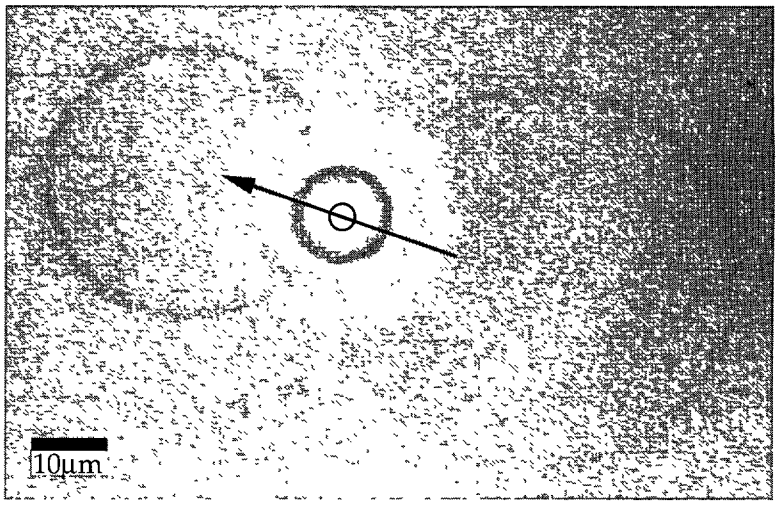

Fig. 9. — Example of a sphere+2 vesicle complex ($a = 6.9$ μm, SOPC, $T = 24$ °C). With the optical trap, we moved the sphere in the direction shown by the arrow. The whole complex reoriented as a rigid body, with the small vesicle ($R = 18$ μm) ahead and the large one ($R = 26.6$ μm) behind the particle.

4.2. PARTICLE INGESTION ②. — In the former paragraph, we described the "adhesion" step, which we characterized by a sudden inward jump of the particle following contact. As we explained, this event does not cause a definite variation of the vesicle radius. The sequence shown in Figure 10 starts with a classical adhesion step (denoted ①), which resulted in a penetration $z_e = 0.2$, with no change in the vesicle radius. However this configuration survived for only a small period (0.16 s in this example). Then the particle made a second jump (denoted ②). We name "particle ingestion" this kind of event, which is distinct from adhesion because it is correlated to a significant decrease of the vesicle radius. We observed ingestion for unilamellar and multi-lamellar vesicles. The time elapsed between adhesion and ingestion may be viewed as the lifetime t_c of the partial wetting configuration. In our experiments with SOPC vesicles, we observed that this lifetime was very large, sometimes beyond experimental time (days), except with very large spheres or pre-tensioned membranes (Fig. 10 is an example of such a situation).

In Figure 8b all cases where adhesion was followed by ingestion are marked by an arrow; each arrow points to the final value of R/R_0, after ingestion. In one example (extreme right) the vesicle "disappeared" ($R/R_0 \to 0$ symbolically). The numerical values corresponding to the five ingestion events observed with SOPC vesicles and one with an "ideal" DMPC vesicle are gathered in Table I. In general ingestion led to complete ($z_f = 2$) or nearly complete ($z_f \geq 1.6$) particle penetration. The Table shows that the apparent wetted area (S_{ad}) is approximately equal to the variation of the vesicle surface area before and after ingestion (ΔS_v). Ingestion happens within few video frames. In the example of Figure 10 it took less than a video period (40 ms). Unfortunately we were not able to resolve the event in time because of the too large excursions of the sphere (the PSD method is restricted to $d < a$). The last column in Table I gives estimated values of the membrane tension (σ) just before the onset of ingestion. To calculate σ, we supposed $A = 1$ erg/cm^2, and just injected the experimental contact angles into equation (1).

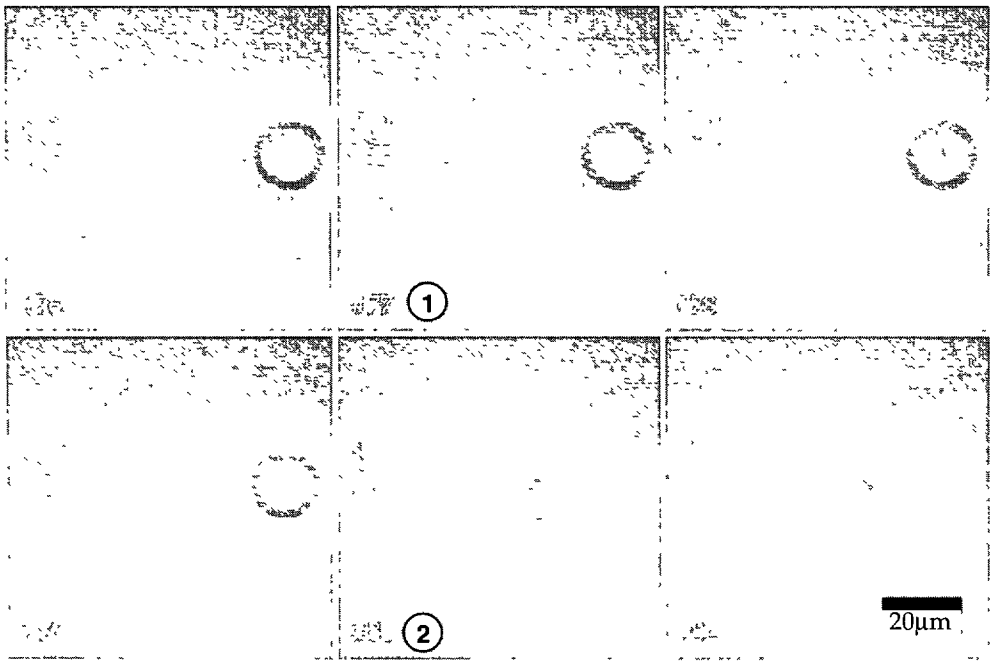

a)

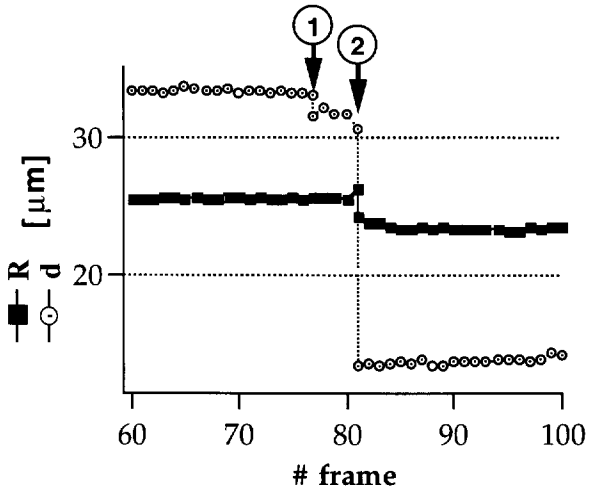

b)

Fig. 10. — a) Video sequence showing a complete penetration of a Latex sphere ($a = 9.2$ μm) into a SOPC vesicle ($R_0 = 26.6$ μm, $T = 24$ °C). This vesicle is part of a "twin configuration", as shown in Figure 9. The Latex sphere between both vesicles is visible at the border of the frames and out of focus. Note that the sequence starts with a partial penetration ①, which stays stable only for 0.16 second. Panel b) gives $R(t)$ (filled squares) and $d(t)$ (circles) for the whole series of recorded frames. The different events (indicated by numbers) during the attachment are described in the text.

Table I. — *Radii and related area of phospholipid vesicles before and after attachment of a Latex sphere. Note that the final penetration value z_e of the sphere can be less than 2.*

	R_0 [μm]	R [μm]	ΔS_v [μm^2]	a [μm]	S_{ad} [μm^2]	t_c [S]	z_f	z_e	σ (theory) [dyne/cm]
SOPC	26.6	23.5	−1325±200	9.2	1066±50	0.2	2	0.16	4.7
SOPC	10.0	-	−1000±200	7.3	670±40	60	-	0.31	2
SOPC	19.0	17.2	−813±100	7.7	743±45	30	2	0.42	1.8
SOPC	13.0	11.8	−389±100	7.0	402±100	15	1.6	0.37	1.9
SOPC	22.4	21.6	−500±100	6.85	471±100	> 60	1.7	0.90	1
DMPC 30 °C	24.9	24.65	−166±80	3.6	163±20	3	2	0.76	1.2

4.3. PARTICLE EXPULSION ③ AND RE-CAPTURE ④. — The situation with an ingested particle is generally stable (*e.g.* for all cases given in Tab. I). The particle stays tangent internally to the vesicle contour. However we observed a destabilization of this configuration in quite a few examples. As shown in Figure 11, the ingested particle can be partly expelled out of the vesicle interior (step ③) and move back in again (step ④). This "expulsion-recapture" sequence ends in a configuration which looks like partial penetration, as in the adhesion step (step ①). Note that steps ③ and ④ are definitely slower than steps ① and ② that the particle radius decreases monotonously between steps ② and ④. We observed that in the final configuration the re-captured sphere was not partially wetted, contrary to what the finiteness of the apparent contact angle might suggest, but probably totally wetted by the lipid material. We went to this conclusion by repeating the procedure to build a two-vesicle sphere complex as in Figure 9. We observed that the outer portion of the re-captured sphere did not adhere on a second vesicle, which means that this part of the solid surface was not "dry" in the sense we defined before. Most probably, the re-captured sphere was fully coated by lipids, as it was after ingestion.

In some experiments, we observed a "condensed" version of the sequence. These experiments were carried out with small spheres ($a/R_0 < 0.1$), as in the example illustrated in Figure 12. The particles penetrated completely inside the vesicle in the first step ①, as one might expect for a small sphere (complete adhesion). Expulsion ③ followed nearly immediately, and the particle was stabilized at a final penetration value z_f ($z_f = 0.4$ for the example of Figure 12, in some cases we observed a complete expulsion $z_f = 0$).

The example shown in Figure 13 is perhaps very particular because the giant vesicle to which the solid sphere was adhered contained a few smaller vesicles. One of them is clearly visible in the video sequence. The particle was ingested about 20 seconds after adhesion and nearly immediately expelled and re-captured. Interestingly, the smaller vesicle was expelled too, at the same time as the Latex sphere.

4.4. FINAL REMARKS

(i) Experimentally the sphere-vesicle configuration after an "ingestion" with $z_f = 2$ was not distinct from an "adhesion" in the complete wetting regime $z_e = 2$. For lipids in the fluid state, we could never detach an ingested (or more generally speaking a fully encapsulated sphere)

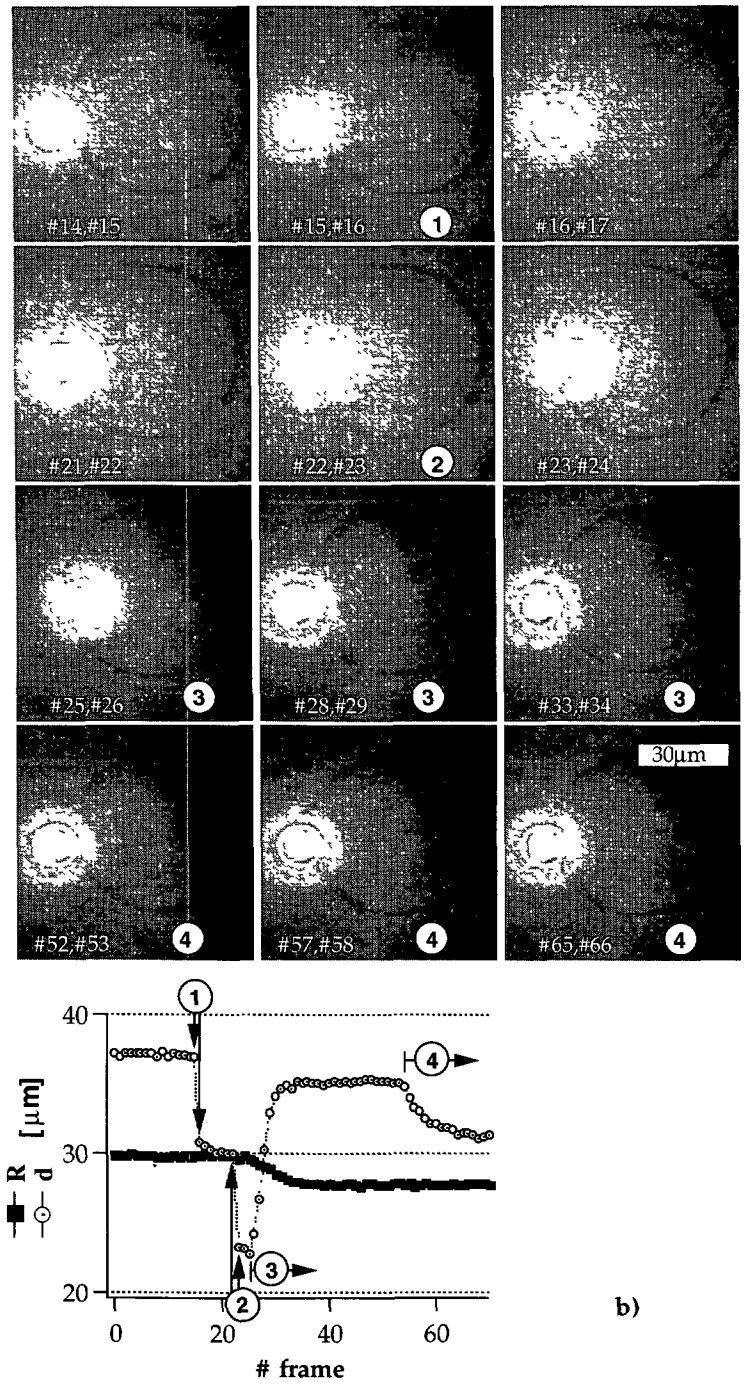

Fig. 11. — Penetration of a Latex sphere ($a = 7.5$ μm) into a DMPC vesicle ($T = 30$ °C). a): Video sequence. Note: To highlight rapid sphere movements we superimposed two successive video frames. Frame numbers are included in every panel. b): $R(t)$ (filled squares) and $d(t)$ (circles). The sequence features the 4-step process: adhesion ①, ingestion ②, expulsion ③ and re-capture ④, which correspond to the different rows of the video micrographs.

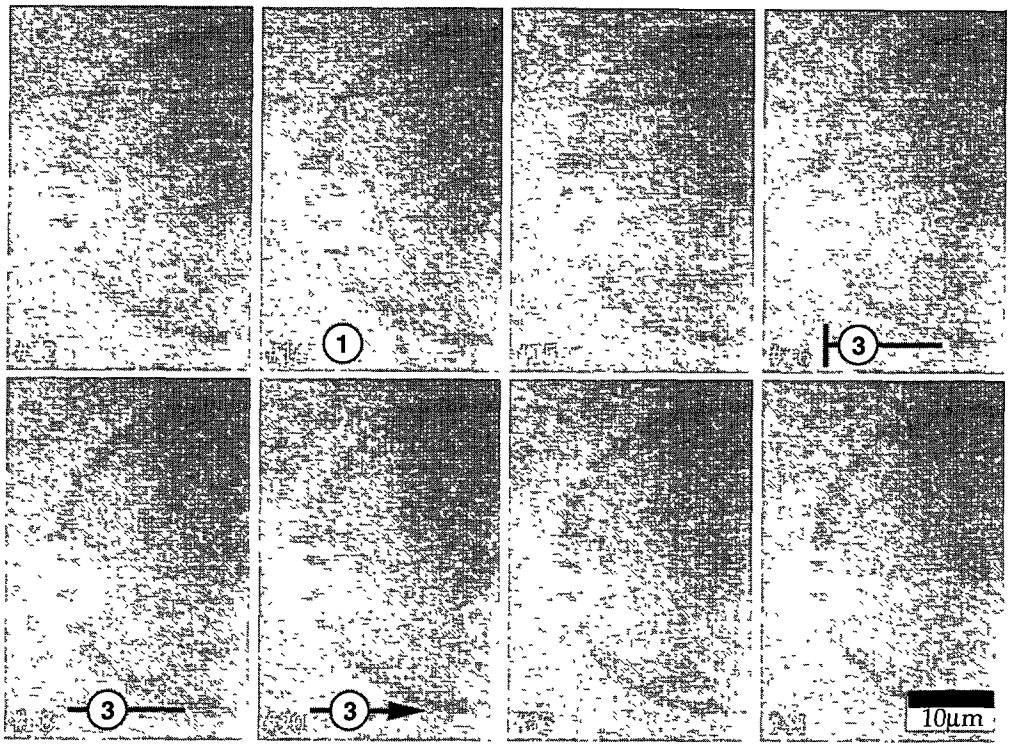

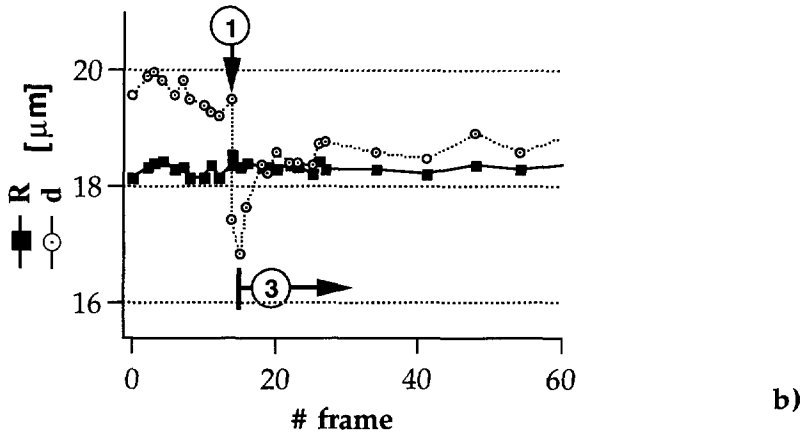

Fig. 12. — a) Small Latex sphere ($a = 1.1$ μm) and DMPC vesicle ($T = 30$ °C): Adhesion ① followed by expulsion ③. Frame numbers are given within each panel. b) $R(t)$ (filled squares) and $d(t)$ (circles) for the whole series of recorded frames.

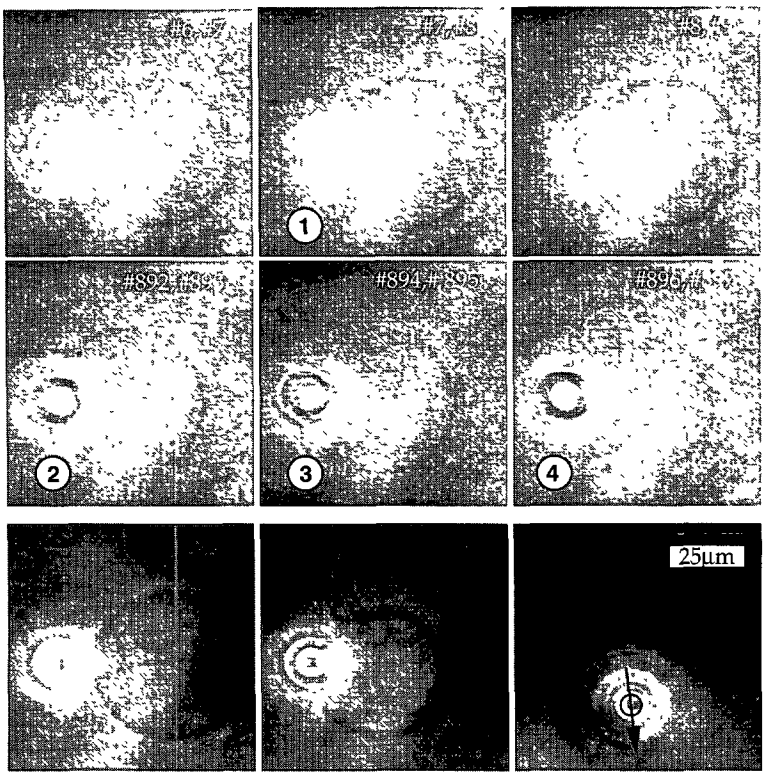

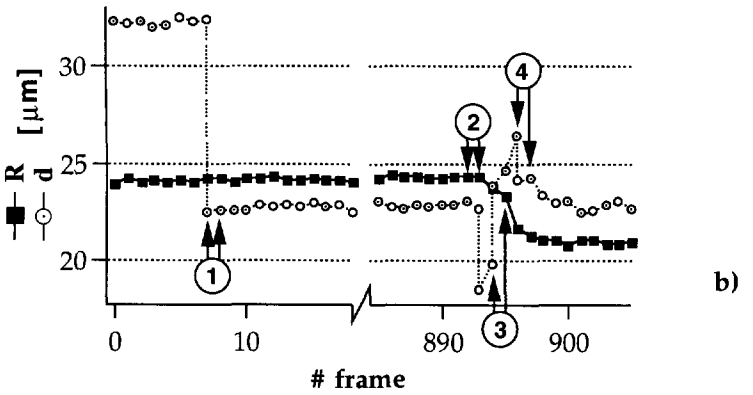

Fig. 13. — Penetration of a Latex sphere ($a = 8$ μm) into a SOPC vesicle ($T = 24$ °C) and subsequent expulsion of an inner vesicle. a) The micrographs in the first two rows are the result of the overlay of two successive frames (corresponding ♯ frame are included). The three last micrographs were obtained by averaging 16 successive video frames and show the vesicle-sphere complex before adhesion, after expulsion of an inner vesicle and when dragging the whole complex with the optical trap in the direction indicated by the arrow. b) $R(t)$ (filled squares) and $d(t)$ (circles) for the whole series of recorded frames. Within the resolution of the image analysis, the radius of the expelled small vesicle stayed unchanged ($R_{\text{small}} = 9$ μm).

Table II. — *Compilation of the different sequences recorded in this work.*

Vesicles	♯ of events with		type of event			
	SOPC	DMPC	adhesion	ingestion	expulsion	re-capture
uni	14	4	•			
lamellar	5	1	•	•		
multi	5	-	•			
lamellar	-	2	•	•		
	2	3	•		•	
	3	2	•	•	•	•

out of the vesicle contour by means of the optical trap ([1]). Thus, we have no direct proof of a physical endocytosis, in the sense of a true disconnection of the internalized particle from the vesicle membrane.

(ii) To conclude this section, we want to give an idea of the statistics of the different processes that we described. The main features of our experiments, in terms of the sequences which were observed, are gathered in Table II. Adhesion of Latex spheres to fluid membranes was observed systematically with all kinds of vesicles, either attached to the electrodes [29] or free, either uni- or multi-lamellar. In a few exceptions, adhesion was impossible, however there were indications that the particles had been contaminated with lipids prior to contact with the vesicle. The adhesion events which are analyzed quantitatively in this article were obtained with "ideal", *i.e.* uni-lamellar and with no indication of internal structures. Ingestion, expulsion and re-capture are not systematic, as we explained. Because of this restriction, the number of experimental realizations in ideal conditions is much smaller than for simple adhesion. Actually, expulsion and re-capture were observed mainly with non ideal vesicles, *i.e.* multi-lamellar or bearing internal structures.

5. Discussion

Our observations about the *adhesion* of Latex spheres to vesicle membranes are qualitatively well in line with the partial wetting model worked out in Section 2.1. As predicted the relative penetration depth increased with decreasing ratios of a/R, the particle portion outside of the vesicle contour was free of lipid and penetration values were shifted to lower and higher values for flaccid or pre-tensioned vesicles, respectively.

For a quantitative analysis we deal with two unknown parameters, namely the adhesion energy (A) and the excess area (ε). We may suppose that A is a constant independent of the particular experiment, but ε certainly takes on different values with different vesicles. In a first step, one may suppose $\varepsilon = 0$ everywhere: this rough statement allows us to find boundaries for the value of A. Indeed, setting $\varepsilon = 0$ leads to over or underestimate A , according to whether the vesicle is flaccid ($\varepsilon > 0$) or pre-tensioned ($\varepsilon \ll 0$). Doing so, we find from the data shown in

([1]) We could observe physical endocytosis in the case of an unilamellar DMPC vesicle at 22.5 °C, near the main phase transition of this lipid ($T_M \sim 24$ °C). After complete penetration the sphere could be brought to the center of the vesicle by optical manipulation. Apparently there was no connection between the internalized particle and the membrane. By "connection", we mean a filament that could be observed optically or could be felt mechanically.

Figure 8 (SOPC): $0.1 < A < 4.5$ erg/cm^2. The solid line in Figure 8 is a theoretical prediction for $\varepsilon = 0$ and $A = 1$ erg/cm^2. This line fits to the points corresponding to initially spherical vesicles, *i.e.* the case where the assumption that $\varepsilon \approx 0$ is most reasonable (these vesicles did not show contour fluctuations and were not pre-tensioned). Of course this value is well within the above-mentioned boundaries.

The model provides no explanation for the irreversibility of lipid membrane adhesion, which we observed as a contact line pinning in the experiments involving a vesicle + 2 spheres or a single sphere attached to two vesicles simultaneously. This suggests that adhesion of lipids on the Latex surface involves two kinds of forces, of which only the first one is accounted for by the phenomenological constant A. The second kind of forces may be contact forces or may be the result of a combined rearrangement of the Latex material and of the lipid bilayer after contact with the membrane. Because of this complication, the model is not directly applicable to a quantitative analysis of the experiments involving two spheres on the same vesicle.

The phenomenon of particle *ingestion* can be understood with the ideas set-out in Section 2.1 too. Though the sphere penetrates into the vesicle, we observe a decrease in the vesicle radius. This is only possible if sizable amounts of water are simultaneously rejected by the vesicle. We interpret ingestion as being due to the onset of membrane rupture. This rupture is commonly attributed to the formation and growth of holes (pores) across the membrane. Values of rupture tension σ_c, about 6 dyne/cm for SOPC and 2 dyne/cm for DMPC, were determined by Evans and Needham [18] by means of the micro aspiration technique. Injecting $A = 1$ erg/cm^2 into equation (1), one deduces the values of the lateral tension after sphere adhesion. The example of Figure 10 (SOPC) thus gives $\sigma = 4.7$ dyne/cm, which is near the rupture threshold σ_c of this species. The other examples in Table I show that in general $\sigma \leq \sigma_c$. Note that values closest to σ_c correspond to short lifetimes t_c, on the order of a second or less. The dispersion in the values of σ may be the manifestation of the stochastic character of membrane failure through pore growth. Basically, membrane rupture may happen under any finite tension. This is just a matter of time. Strictly speaking, the rupture tension cannot be defined independently of the membrane lifetime. In our situation, pore growth did not lead to vesicle destruction in general (1 exception with a SOPC vesicle, see Fig. 8b). The occurrence of a hole across the membrane increases the permeation rate of the water out of the vesicle. This outflow relaxes the membrane tension; which makes the vesicle survive. This kind of phenomenon has much in common with the one described by Zhelev and Needham, in the case of pipette held vesicles and electrically induced pores [13]. These experiments and ours are technically very different, but both of them are based on membrane tensioning, either by suction through a pipette or by membrane adhesion on a solid sphere. Analysis of the experimental dynamics by means of an appropriate model should provide basic information about pore line tension and growth [30].

The simple picture of the membrane acting as a mere elastic film that adheres to the solid surface turns out correct, as far as adhesion and ingestion are concerned. At the molecular level, this means that the lipid bilayer feels the Latex sphere surface as "hydrophilic", *i.e.* with molecule polar heads directed inward to the solid surface (Fig. 14a). This view is also supported by the result that the loss of membrane area after an ingestion event fits well to S_{ad} (*cf.* Tab. I). This picture may be surprising, because the major part of the Latex surface is "hydrophobic" and thus one might expect a "tail-in" configuration of the lipids (Fig. 14b) to be energetically favorable. Actually, adsorption experiments on lattices seem to support this view [31–33]. We believe that the first scheme (Fig. 14a) is metastable. The configuration of Figure 14b is not forbidden *a priori*, but needs complex processes to take place such as lipid reorientation (flip-flop) or sliding of the monolayers relative to each other. Note that the situation is different in adsorption experiments with surfactants, since these are in solution. These processes are probably much to slow to play a role in our systems.

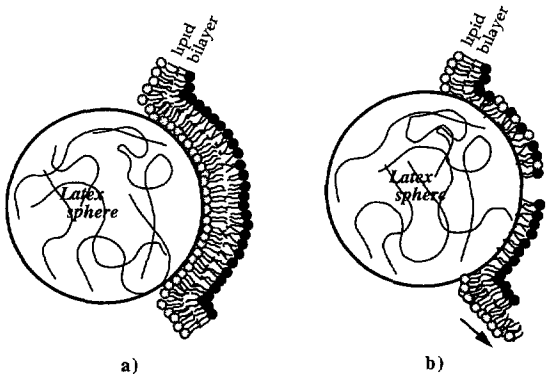

Fig. 14. — The so-called "hydrophilic" (panel a) and "hydrophobic" (panel b) scenario for the adhesion of a lipid bilayer to a solid surface. For clarity, the bilayer thickness is considerably enlarged. The molecules are "colored" in gray and black, to keep track of which monolayer they come from.

This point is supported by the result of experiments which we performed with decane micro droplets and SOPC vesicles (data not shown). These experiments showed no adhesion of the lipid membrane on the water/oil interface and no alteration of the vesicle shape, even when contact was maintained for several minutes. From this, we draw a two-fold conclusion: (i) the tail-in configuration (Fig. 14b), which is the obvious equilibrium configuration in the case of the oil-water interface, is not realized within at least minutes; (ii) the ionic groups on the surface of the Latex beads probably play the role of binding sites for the membrane on the Latex surface. To summarize, the head-in configuration (Fig. 14a) corresponds to a minimum in the energy of the membrane solid system. The tail-in configuration (Fig. 14b) is likely to have a lower energy, but is out of reach within our experimental time (minutes) because of a very high energy barrier.

Up to this point, the discussion was restricted to equilibrium states (energy minima). We now come to the *kinetic* aspects of the particle membrane interaction. The model set-out in paragraph 2.2 yields an estimate of the encapsulation time in the millisecond range, *i.e.* within the experimental range ($\tau_{\rm enc} \approx 4$ ms in the example of Fig. 7c). However, the theoretical $d(t)$ does not fit to the experimental one, as visible in Figure 7c. The experimental particle velocity jumps abruptly from zero to about 1 μm/s at the onset of encapsulation ($z = 0^+$). This is in contrast to the theory, which predicts a vanishingly small initial velocity, independently of the values of A and ε. This feature is the consequence of the divergence of the dissipated power when $z \to 0$, as we explained. Apparently, the experimental record suggests that the friction when $z = 0+$ is finite.

Interestingly, the experimental kinetics can be recovered if we make the naive assumption that the friction force acting on the particle is just proportional to its velocity:

$$f_{\rm fr} = -\dot{z} a \xi. \tag{23}$$

Here ξ is a phenomenological friction coefficient. If we neglect inertia or other forces sensed by the sphere, the friction force is balanced by the adhesion ($f_{\rm ad}$) and elastic ($f_{\rm el}$) forces. Thus:

$$\dot{z} = \frac{f_{\rm el} + f_{\rm ad}}{a\xi}. \tag{24}$$

The encapsulation trajectory is obtained by numerical integration of equation (24).

As in paragraph 2.2, we compute the distance $d(t) = d(0) - z(t)a$ using the same numerical procedure as before (Appendix B), and with the same values of a, R_0, A and ε. We find that the computed trajectory best fits to the experimental one (open circles) for $\xi = 3.6$ g/s, *i.e.* about 250 times the Stokes value for the same sphere in bulk water. For the sake of rigor, we also included inertia and radiation pressure forces in equation (24), and found that these had a negligible impact on the solution (inertia makes the acceleration finite at $z = 0^+$, but this is not visible in the graph).

Basically, setting ξ = constant in equation (24) is just an *ad hoc* assumption, which amounts to supposing that P is simply proportional to $\eta a^3 \dot{z}^2$, in contrast to the more complex but physically supported behavior represented by equation (18). The success of the *ad hoc* model suggests that the way in which the membrane progressively wets the particle surface might be different from the simple picture sketched in Figure 1b. For instance, the particle surface could be non uniform in terms of adhesion sites density. This would result in a non plane contact line and, consequently, make the flow fields, in the membrane and in the surrounding water, very different from the idealized (axis-symmetric) picture which we supposed up to now. In fact, contact line pinning is already an indication that Latex particles surfaces are not uniform. Beside this, we also observed situations where the membrane flow field was clearly non axis-symmetric, and even that the particle would rotate during the encapsulation process ([2]). Of course, these complications make any accurate computation of the encapsulation kinetics an elusive goal. In this regard, the adequateness of the *ad hoc* model is the result — paradoxically — of the complexity of the particle surface. Here we have to admit that we essentially set out — hopefully — interesting problems, rather than solutions.

We have no serious explanation for the phenomena of particle *expulsion* and *re-capture*. We can just speculate that a membrane rupture happens at the level of the connection between the sphere and the vesicle contour after ingestion. When the sphere is completely covered, it may follow the water outflow and be pushed out of the vesicle. Again tension will decrease definitely and the hole will heal. As we explained in Section 4, the outer portion of the sphere in the final configuration is wetted by lipids. This particularity was already noticed in early experiments with vesicles connected to the lipid cluster [29], and a simple scheme was proposed to explain the full particle encapsulation by a single bilayer with a finite contact angle [34]. This scheme remains possible. Nevertheless, we cannot rule out that the particle be located between different bilayers. The situation is complicated by the fact that for nearly all cases of expulsion and re-capture, there were clear indications that the vesicles were not unilamellar.

([2]) Our model assumes a cylindrical symmetry around the particle axis. The movement of the particle is a pure translation towards the vesicle center, and that of the membrane is purely radial (the flow anywhere in the membrane depends only on the distance to the axis). Some of our observations were carried out with markers attached to the membrane at some distance from the large Latex particle. These markers were sometimes just accidental, in the form of little lipid structures, or in the form of a couple of little (2 μm) Latex particles which we purposely adhered to the vesicle. Experiments showed that the markers did not move radially as a whole, but rotated; which means that the membrane was sheared. We performed a few experiments with markers on the particle surface too: again we took advantage of an accidental situation where a small particle went stuck to the large one in the Latex suspension. We used this complex which we adhered to a vesicle, with the marker on the side opposite to the vesicle. During the adhesion step, the marker was seen to rotate, about 90°.

6. Conclusion

We used optical manipulation to study the interaction between polystyrene spheres, a few microns in size, and giant lipid vesicles whose membranes (SOPC or DMPC) were in the fluid state. We showed that the interaction proceeds through different well-established steps, namely adhesion, ingestion and sometimes expulsion and re-capture. Adhesion starts when the sphere surface gets in contact with the membrane. Ingestion of the particle occurs when the increase of membrane tension due to adhesion is large enough to generate a pore of macroscopic size across the membrane.

The observations about *adhesion* and *ingestion* are well-explained by the model set-out in Section 2. This model deals with a strong adhesion regime. The tendency of the membrane to increase its contact area to the solid sphere is counterbalanced by the elastic stretching of the lipid lamella. The interfacial tension is not a constant, which is an essential difference from the classical partial/total wetting problem. As a consequence, the contact angle depends on the particle/size ratio and on the initial membrane tension, in a way which is confirmed by experimental observations. This agreement allowed us to estimate the adhesion energy of the studied membrane on the polystyrene beads, $A \approx 1$ erg/cm^2, and led to the view that the Latex bead surface is essentially felt as "hydrophilic" by the lipid bilayer. The observed kinetics of the adhesion step could be modeled within this scenario.

Particle *expulsion* and *re-capture* is a spectacular process which ends up with the particle across the vesicle contour, as in the adhesion step. However, we showed that the re-captured particle was totally wetted by lipids, contrary to what the finiteness of the membrane-solid surface contact angle might suggest. This configuration is the result of a complex series of events, whose interpretation is still speculative.

Essentially, the work presented in this paper was aimed at understanding the particle position and movement in the radial direction, *i.e.* towards the vesicle center. In this context, the laser trap was used just to bring a particle in contact with a vesicle, sometimes to convey a vesicle-particle complex. As we explained, there is no influence of the laser beams on the adhesion process and on the position of the particle relatively to the membrane ([3]) [35–37].

In our analysis, the main characteristic of the sphere-membrane configuration was the particle penetration degree into the vesicle contour, and the way in which this quantity depends on the vesicle and sphere sizes. Optical manipulation allowed us to gain some more information about the repartition of the lipid material on the part of the sphere outside of the vesicle, by mechanical probing. Incidentally, we made a few attempts to observe this repartition directly with the help of fluorescent markers located in the membrane. For simplicity, we chose a dye that could be excited by the green light of the laser trap ("Texas Red", Molecular Probes). Unfortunately, the fluorescence signal at the instant of adhesion was too weak and short-lived to be recorded. Probably, bleaching of the dye by the intense laser radiation was the cause of the problem. Ideally, the wavelength of the laser trap should be different from those of fluorescence excitation and emission. We hope to solve this technical problem in the future.

From a different point of view, Latex spheres can be used to perform well-defined manipulations on lipid vesicles. Using them as a hook to transport vesicles or as a glue to fix them at a desired place opens a wide field of preparational possibilities. Indeed this gives the basis to create a well-defined environment to look at the movement of particles when attached to

([3]) There is no direct influence of the laser beams on the vesicle membrane in our conditions. Direct effects are visible with beams which are tightly focused (power density $> 10^6$ W/cm^2) on membranes under very weak (driven by undulations) tensions. See: [35–37] and references therein. In our experiments, power densities are moderate ($< 10^5$ W/cm^2) and tensions are in the "mechanical" range (on the order of 1 dyne/cm).

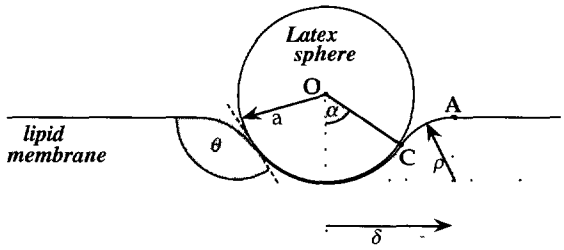

Fig. 15. — Bending of the membrane near to the membrane-solid sphere contact line.

a lipid membrane. For a fluid lipid membrane the particle is free to move along the vesicle surface. The movement can be thermally excited (Brownian motion) or driven by an external force like gravity or radiation pressure. The particle motion is characterized by a diffusivity or a friction, whose values depend on the membrane viscosity. In this context, the microsphere plays the role of a little surface viscosimeter, as in the recent experiments of Petkov *et al.* [38]. A similar analysis can be done with two or even more particles attached to a same vesicle. Preliminary experiments of this kind already showed the existence of striking long range interactions between the particles [29]. Membrane viscosimetry and the study of membrane mediated interactions between microspheres are currently in progress in our laboratory.

Appendix A

Contact Line Energy

We consider the situation sketched in Figure 15. The vesicle radius is very large ($R_0 \gg a$). In the region of the contact line, the membrane is supposed to follow a toroidal shape, between points A and C in the cross-section of Figure 15. C is the true membrane-sphere contact point. We denote ρ the radius of the tore cross section. The angle α defined in Figure 15 is simply related to the contact angle by $\theta = \pi - \alpha$.

In the analysis worked out in Section 2 in the limit $R_0 \gg a$, $z = 1 - \cos\alpha$ was the only variable in the energy of the system. Now we have to handle two variables, namely α and ρ. The goal of this appendix is to estimate the value of ρ at equilibrium and the importance of the toroidal portion of the membrane in the total energy. We must calculate $E_{\rm el}$, $E_{\rm ad}$ and $E_{\rm l}$. We have:

$$S_{\rm ad} = 2\pi a^2(1 - \cos\alpha) \tag{A.1}$$

$$S - S_0 = S_{\rm ad} + S_{\rm T} - \pi\delta^2 - 4\pi R_0^2\varepsilon \tag{A.2}$$

$S_{\rm T}$ is the area surface area of the above defined tore portion and

$$\delta = (a + \rho)\sin\alpha \tag{A.3}$$

is the distance between A and the symmetry axis. $S_{\rm T}$ is given by

$$S_{\rm T} = 2\pi[(a + \rho)\rho\alpha\sin\alpha - (1 - \cos\alpha)\rho^2]. \tag{A.4}$$

Equation (A.1−A.4) allow us to calculate $E_{\rm ad} + E_{\rm dil}$. The line energy $E_{\rm l}$ is due to the curvature of the membrane in the contact region. The general expression of the curvature energy involves the constants $k_{\rm c}$ and $\bar{k}_{\rm c}$ (mean and Gaussian curvature elasticity constants) and is rather

complex in the geometry of interest. Fortunately it simplifies considerably if we assume $\rho \ll \delta$. Actually, we expect this condition to be satisfied if the sphere size is not too small and if the adhesion energy is large enough to produce a significant penetration. Indeed, this is so in our experiments, and we will verify that our results are consistent with this view. This simplification leads to

$$E_l = E_c \approx k_c \frac{S_T}{\rho^2}. \tag{A.5}$$

From the explicit expressions of the surface areas, we find:

$$E_{el} \approx k_a \frac{\pi a^4}{8R_0^2}\left[(1-\cos\alpha)^2 + 2\frac{\rho}{a}(\cos^2\ \theta - 1 + \theta\ \sin\theta) - 4\varepsilon\left(\frac{R_0}{a}\right)^2\right] \tag{A.6}$$

$$E_{ad} = -2\pi A a^2(1-\cos\alpha) \tag{A.7}$$

$$E_l \approx 2\pi k_c(a/\rho)\alpha\sin\alpha. \tag{A.8}$$

Minimization of $E_{ad} + E_{dil} + E_l$ as a function of ρ leads to:

$$\frac{a^2}{\rho^2} = \frac{k_a}{k_c}\ \frac{a^4}{4R_0^2}\ \frac{\cos^2\ \alpha - 1 + \alpha\sin\alpha}{\alpha\sin\alpha}. \tag{A.9}$$

Thus we estimate

$$\rho \approx \frac{2R_0}{a}\sqrt{\frac{k_c}{k_a}}. \tag{A.10}$$

With $R = 30\ \mu$m, $a = 8\ \mu$m, $k_c = 4\times10^{-13}$ erg/cm^2, $k_a = 200$ erg/cm^2, we find $\rho \approx 5$ nm, a value on the order the membrane thickness, *i.e.* near the physical lower limit of ρ. This result is obviously consistent with our assumption that $\rho \ll a$.

Note that ρ can be expressed as a function of the membrane tension:

$$\rho \approx \sqrt{\frac{k_c}{\sigma}} \tag{A.11}$$

in agreement with Evans estimate [5].

To estimate the importance of line energy in the total energy of the system, we regard E_l as a perturbation of $E_{ad} + E_{dil}$. The minimum value of the unperturbed $(E_{ad} + E_{dil})$ is equal to $\frac{-3\pi}{8}k_s a^4 R_0^{-2}$ (for $\varepsilon = 0$). Then, using (A.10) and (A.11), we find:

$$\frac{E_l}{E_{el} + E_{ad}} \approx \frac{8}{3}\ \frac{R_0}{a^2}\sqrt{\frac{k_c}{k_a}}. \tag{A.12}$$

With the same numerical values as before, the above ratio is found $\approx 10^{-3}$ Thus, the line energy is negligible in our conditions. This would not be true with much smaller spheres. With the same values of the vesicle radius, we find a crossover size of about 0.1 μm.

Appendix B

Numerical Procedure (Section 2)

In this appendix, we give the main equations which we used to calculate the sphere-vesicle interpenetration in the general case, *i.e.* for arbitrary values of the size ratio (a/R). Our calculation spans the domain between $a/R \to 0$ (Fig. 1b) and $a/R \to \infty$ (Fig. 1c). The former

limit is dealt with analytically in Section 2. The latter limit corresponds to the more classical problem of a vesicle that adheres to a flat substrate [5]. The interpenetration za is the sum of the quantities s and v defined in Figure 1a:

$$za = s + v. \tag{B.1}$$

The condition of volume conservation is expressed as:

$$\frac{4}{3}\pi R^3 = \frac{4}{3}\pi R_0^3 + \frac{\pi}{3}\left[v^2(3R - v) + s^2(3a - s)\right]. \tag{B.2}$$

(B.1) and (B.2) give:

$$v = \frac{az(2a - za)}{2[R + a(1 - z)]} \qquad s = \frac{az(2R - za)}{2[R + a(1 - z)]}. \tag{B.3}$$

Volume conservation can be reformulated in terms of R and z. We arrive at a homogeneous 4th degree equation:

$$16R^4 + 16a(1 - z)R^3 + 4[a^3(z^3 - 3z^2) - 4R_0^3]R + a[16R_0^3\, z + 4a^3z^3 - 16R_0^3 - a^3z^4] = 0. \tag{B.4}$$

The contact area is equal to $2\pi as$. Then:

$$E_{\text{ad}} = -2\pi Aas. \tag{B.5}$$

The surface extension is simply:

$$S - S_0 = 4\pi R^2 - 4\pi R_0^2 + 2\pi as - 2\pi R\, v - \varepsilon 4\pi R_0^2 \tag{B.6}$$

and

$$E_{\text{el}} = \frac{\pi}{2}k_{\text{a}}\left(\frac{as - Rv - 2\varepsilon R_0^2}{R_0}\right)^2 \tag{B.7}$$

Using (B.3) we obtain an expression of the total energy $E = E_{\text{ad}} + E_{\text{el}}$ as a function of z and R. We first solved (B.4) numerically for R and injected the solution $R(z)$ into E_{ad} and E_{el}. Minimizing $E(z, R(z))$ provides the equilibrium value z_{e}. The elastic and adhesion forces were gained by numerical derivation of $E_{\text{ad}}(z, R(z))$ and $E_{\text{el}}(z, R(z))$ with respect to z. The equilibrium value z_{e} was then found from the intersection of $f_{\text{ad}}(z)$ and $-f_{\text{el}}(z)$ graphs, as illustrated in Figure 2.

To test our results, we checked that the calculated solution satisfied the Young equation (see Fig. 16). In correspondence to equation (7), equation (B.8) gives the general relation of the contact angle θ to the penetration value z

$$z\left[1 + \frac{a}{R}\left(1 - \frac{z}{2}\right)\right] = 1 + \cos\,\theta. \tag{B.8}$$

At the transition point between partial and complete wetting, the procedure reproduced the transition tension $\sigma* = A/2$ as demanded by the Young equation (*cf.* plots of σ in Fig. 3). Furthermore the numerical procedure described the behavior of z_{e} and σ found analytically in the limits $a/R \to 0$ and $a/R \to \infty$ (see Fig. 16).

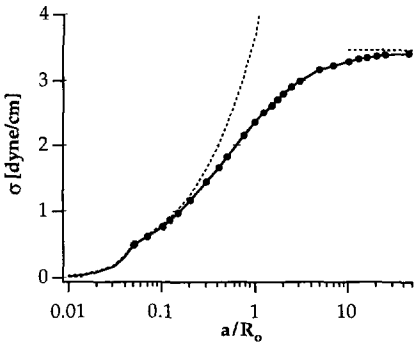

Fig. 16. — Example of a numerically computed (σ, a/R_0) graph, from $a/R_0 \ll 1$ up to $a/R_0 \gg 1$. Input parameters are $k_a \simeq 200$ dyne/cm, $A = 1$ erg/cm^2, $\varepsilon = 0$. The dotted lines are the asymptotic behaviors, in the $a \to \infty$ and $R_0 \to \infty$ limits. The markers represent the lateral tension calculated from the Young equation (Eq. (1)) by injecting the numerically determined penetration depth.

Acknowledgments

This work was supported by the "Laboratoire franco-bulgare" (CNRS/Bulgarian Academy of Sciences), by Ultimatec program (CNRS) and by the Bulgarian National Science Foundation (Project K-437/94). One of us (C.D.) acknowledges an 11-month fellowship from the European Union. We thank D. Bensimon, P. Bothorel, Y. Chevalier, P. Kralchevsky, K. Lunkenheimer, G. Martinot-Lagarde, P. Méléard, R. Merkel, J. Prost, P. Richetti, F. Rondelez for illuminating discussions.

References

[1] Angelova M.I. and Dimitrov D.S., *Prog. Colloid Polymer Sci.* **76** (1988) 59-67.
[2] Angelova M.I., Soléau S., Mélárd P., Faucon J.F. and Bothorel P., *Springer Proc. Phys.* **66** (1992) 178-182.
[3] Seifert V. and Lipowsky R., *Phys. Rev. A* **42** (1990) 4768-4771.
[4] Evans E., *Colloids Surf.* **43** (1990) 327-347.
[5] Evans E., *Adv. Colloid Interface Sci.* **39** (1992) 103-128.
[6] Rädler J., Feder T., Strey H. and Sackmann E., *Phys. Rev. E* **51** (1995) 4526-4536.
[7] Helm C.A., Israelachvili J.N. and McGuiggan P.M., *Science* **246** (1989) 919-922.
[8] Servuss U. and Helfrich W., *J. Phys. France* **50** (1989) 809-827.
[9] Guiot P. and Couvreur P., Polymeric Nanoparticles and Microspheres, P. Guiot and P. Couvreur, Eds. (Boca Raton, Florida, CRC Press, 1986).
[10] Bo L. and Waugh R.E., *Biophys. J.* **55** (1989) 509-517.
[11] Evans E., Ritchie K. and Merkel R., *Biophys. J.* **68** (1995) 2580-2587.
[12] Velikov K., Master of Science, University of Sofia (1996).
[13] Zhelev D.V. and Needham D., *Biochim. Biophys. Acta* **1147** (1993) 89-104.
[14] Ivanov I.B., Dimitrov A.S., Nikolov A.D., Denkov N.D. and Kralchevsky P.A., *J. Colloid Interface Sci.* **151** (1991) 446-461.

[15] Dimitrov A.S., Nikolov A.D., Kralchevsky P.A. and Ivanov I.B., *J. Colloid Interface Sci.* **151** (1991) 462-476.
[16] Aveyard R. and Clint J.H., *J. Chem. Soc. Faraday Trans.* **91** (1995) 175-176.
[17] Evans E. and Rawicz W., *Phys. Rev. Lett.* **64** (1990) 2094-2097.
[18] Evans E. and Needham D., *J. Phys. Chem.* **91** (1987) 4219-4228.
[19] de Gennes P.G., *Rev. Mod. Phys.* **57** (1985) 827-863.
[20] Léger L. and Joanny J.F., *Rep. Prog. Phys.* (1992) 431-486.
[21] Charles G.E. and Mason S.G., *J. Colloid Interface Sci.* **15** (1960) 236-267.
[22] Martinot-Lagarde G., Thesis, Bordeaux I University (1995).
[23] Buican T.N., Neagly D.L., Morrison W.L. and Upham B.W., *New Technol. Cytometry SPIE* **1063** (1989) 190-197.
[24] Angelova M.I. and Pouligny B., *Pure Appl. Opt. A* **2** (1993) 261-276.
[25] Ashkin A., Dziedzic J.M., Bjorkholm J.E. and Chu S., *Opt. Lett.* **11** (1986) 288-290.
[26] Martinot-Lagarde G., Pouligny B., Angelova M.I., Gréhan G. and Gouesbet G., *Pure Appl. Opt.* **4** (1995) 571-585.
[27] Ren K.F., Gréhan G. and Gousbet G., *Opt. Commun.* **108** (1994) 343-354.
[28] Press W.H., Flannery B.P., Teukolsky S.A. and Vetterling W.T., Numerical Recipes: The art of computing, (Cambridge University Press, 1989) pp. 554-560.
[29] Angelova M.I., Pouligny B., Martinot-Lagarde G., Gréhan G. and Gouesbet G., *Progr. Colloid Polym. Sci.* **97** (1994) 293-297.
[30] Moroz J. and Nelson P., *Biophys. J.* **72** (1997) 2211-2216.
[31] Carmona-Ribeiro A.M. and Herrington T.M., *J. Colloid Interface Sci.* **156** (1993) 19-23.
[32] Macdonald P.M., Yue Y. and Rydall J.R., *Langmuir* **8** (1992) 164 -168.
[33] Piirma I. and Chen S.R., *J. Colloid Interface Sci.* **74** (1980) 90-102.
[34] Pouligny B., Martinot-Lagarde G. and Angelova M.I., *Progr. Colloid. Polym. Sci.* **98** (1995) 280-283.
[35] Bar-Ziv R. and Moses E., *Phys. Rev. Lett.* **73** (1995) 1392-1395.
[36] Granek R. and Olami Z., *J. Phys. II France* **5** (1995) 1348-1370.
[37] Goldstein R., Nelson P., Powers T. and Seifert U., *J. Phys. II France* **6** (1996) 767-796.
[38] Petkov J., Danov K. and Denkov N., *Langmuir* **12** (1996) 2650-2653.